Mon. Not. R. Astron. Soc. **000**, 1–18 (2010) Printed 18 January 2010 (MN LATEX style file v2.2)

On the nature of the Milky Way satellites

Yang-Shyang Li[1⋆], Gabriella De Lucia[2] and Amina Helmi[1]
[1]*Kapteyn Astronomical Institute, University of Groningen, P.O. Box 800, 9700 AV Groningen, the Netherlands*
[2] *INAF - Astronomical Observatory of Trieste, via G.B. Tiepolo 11, I-34143 Trieste, Italy*

18 January 2010

ABSTRACT
We combine a series of high-resolution simulations with semi-analytic galaxy formation models to follow the evolution of a system resembling the Milky Way and its satellites. The semi-analytic model is based on that developed for the Millennium Simulation, and successfully reproduces the properties of galaxies on large scales, as well as those of the Milky Way. In this model, we are able to reproduce the luminosity function of the satellites around the Milky Way by preventing cooling in haloes with $V_{\rm vir} < 16.7\,{\rm km\,s^{-1}}$ (i.e. the atomic hydrogen cooling limit) and including the impact of the reionization of the Universe. The physical properties of our model satellites (e.g. mean metallicities, ages, half-light radii and mass-to-light ratios) are in good agreement with the latest observational measurements. We do not find a strong dependence upon the particular implementation of supernova feedback, but a scheme which is more efficient in galaxies embedded in smaller haloes, i.e. shallower potential wells, gives better agreement with the properties of the ultra-faint satellites. Our model predicts that the brightest satellites are associated with the most massive subhaloes, are accreted later ($z \lesssim 1$), and have extended star formation histories, with only 1 per cent of their stars made by the end of the reionization. On the other hand, the fainter satellites tend to be accreted early, are dominated by stars with age > 10 Gyr, and a few of them formed most of their stars before the reionization was complete. Objects with luminosities comparable to those of the classical MW satellites are associated with dark matter subhaloes with a peak circular velocity $\gtrsim 10\,{\rm km\,s^{-1}}$, in agreement with the latest constraints.

Key words: galaxies: dwarf – galaxies: formation – Local Group – cosmology: theory – dark matter

1 INTRODUCTION

The satellites of the Milky Way (MW) are powerful touchstones for galaxy formation and evolution theories. Their proximity facilitates detailed observations and characterisation of their properties and hence constrains 'near-field' cosmology. In addition, their shallow potential wells make them more sensitive to astrophysical processes such as supernova (SN) feedback (Larson 1974; Dekel & Silk 1986) or to the presence of a photoionization background (Babul & Rees 1992).

Deep images have allowed the construction of colour-magnitude diagrams (CMD) of the MW satellites, from which the star formation histories have been deduced. These studies indicate that there is a large variety in the star formation histories of these galaxies (Mateo 1998; Dolphin et al. 2005). The two gas-rich dwarf irregular (dIrr) Magellanic Clouds show on-going star formation while the other dwarf spheroidal galaxies (dSphs) are gas-deficient and show generally little evidence for recent star formation. Modern studies have revealed that all satellites contain an old stellar population (> 10 Gyr), which likely keeps the imprints of the young Universe.

In recent years, the number of known satellites around the MW has doubled, thanks to the discovery of very low surface brightness dwarf galaxies in the Sloan Digital Sky Survey (SDSS) (Willman et al. 2005a,b; Belokurov et al. 2006, 2007; Zucker et al. 2006a,b; Irwin et al. 2007; Walsh et al. 2007; Belokurov et al. 2008, 2009). Since the sky coverage of SDSS DR5 is about 1/5 of the full sky and the surface brightness limit is about $\mu \sim 30\,{\rm mag\,arcsec^{-2}}$ (Koposov et al. 2008), many satellites are likely yet to be discovered in the next generations of surveys. E.g. Tollerud et al. (2008) have used sub-samples of the Via Lactea I (Diemand et al. 2007) subhaloes to conclude that the total number of MW satellites within 400 kpc should be between ∼300 and ∼600 and dominated by satellites fainter than $M_V = -5$.

The new SDSS satellites have lower surface brightness ($\mu > 27\,{\rm mag\,arcsec^{-2}}$) compared to the classical satellites, but similar physical sizes. They have comparable luminosities to some Galactic globular clusters, but are significantly bigger (Belokurov et al. 2007). The nature of these newly discovered satellites is still unclear. They could be the prolongation towards fainter luminosities of the classical MW satellites (Kirby et al. 2008), tidal features (e.g.

⋆ Email: ysleigh@astro.rug.nl

Hercules dSph, Coleman et al. 2007; Sand et al. 2009), or represent a completely new class of objects.

Kinematic modelling based on line-of-sight velocity dispersions, have demonstrated that the classical MW satellites are dominated by dark matter (Mateo et al. 1993; Mateo 1998). Recent studies have shown that, under the assumption of virial equilibrium, the ultra-faint satellites have mass-to-light ratios as high as $\sim 100-1000$, implying that these objects are the most dark matter dominated systems known (e.g. Muñoz et al. 2006; Simon & Geha 2007). The constraint on the total mass inferred by velocity dispersions is still uncertain because of the mass-velocity anisotropy degeneracy and of the small number of tracers employed in these studies. Recent analyses suggest that the MW satellites (including the newly discovered SDSS satellites) have a common mass scale when considering their innermost regions within 600 or 300 pc (Strigari et al. 2007, 2008).

The cold dark matter (CDM) hierarchical paradigm successfully explains the large scale structures of the Universe (Spergel et al. 2007). Semi-analytic (hereafter SA) galaxy formation models coupled with merger trees extracted from N-body simulations, represent a useful technique to diagnose the complex physics involved in galaxy formation, with modest computational costs. In recent years, SA models have been proved to successfully reproduce a number of observational measurements (e.g. spatial and colour-magnitude distributions) for galaxies seen in the local Universe and at higher redshift (for a recent review, see Baugh 2006). In spite of the encouraging progress on the large scale, however, CDM still faces severe challenges on the galaxy-scale and below. An example is the 'missing satellites problem': namely the substructures resolved in a galaxy-size DM halo significantly outnumber the satellites observed around the MW (Klypin et al. 1999; Moore et al. 1999). A number of studies have suggested that astrophysical processes such as the presence of a photoionization background might reconcile this discrepancy (e.g. Kauffmann et al. 1993; Bullock et al. 2000; Benson et al. 2002; Somerville 2002), without invoking modifications on the nature of the DM particles to reduce the power on small scales of the power spectrum (Kamionkowski & Liddle 2000; Zentner & Bullock 2003).

Several groups have recently attempted to model the properties of the MW and its satellites in a (semi-)cosmological setting. For example, Kravtsov, Gnedin & Klypin (2004) have analysed the dynamical evolution of substructures in high-resolution N-body simulations of MW-like haloes and suggested that all the luminous dwarf spheroidals in the Local Group are descendants of the relatively massive ($\sim 10^9\,\mathrm{M}_\odot$) high-redshift haloes, which were not significantly affected by the extragalactic ultraviolet radiation. Font et al. (2006) have successfully reproduced the observed chemical abundance pattern of the MW stellar halo by combining mass accretion histories of galaxy-size haloes with a chemical evolution model for individual satellites. It should be noted that in these studies, the phenomenological recipes adopted for star formation and feedback have been tuned to reproduce some of the properties of the satellites in the Local Group.

Benson et al. (2002) have used a SA model which successfully reproduces the present-day field galaxy luminosity function to study the properties of dwarf satellite galaxies known at the time. Their model calculates the influence of reionization self-consistently, based on the production of ionizing photons from stars and quasars, and the reheating of the intergalactic medium. This same model reproduces quite nicely the luminosity and size distributions, gas content and metallicity of the classical satellites of the MW and M31. These authors have suggested that the surviving satellites are those which formed while the Universe was still neutral. This study was carried out before the boost at the faint end of the satellite luminosity function. Although they did predict a large number of faint satellites below $M_V = -5$, after extrapolating their prediction on the luminosity-size space to the faint end, Benson et al.'s faint satellites tend to be too small at a given absolute magnitude compared to the ultra-faint satellites discovered in SDSS (Koposov et al. 2008). More recent studies have turned their attention to the ultra-faint satellites: Macciò et al. (2009) have used three different SA galaxy formation models to study the satellite population of MW-like galaxies. They have used both analytic and numerical merging histories of MW-like haloes and shown that all three models reproduce the luminosity function of the MW down to $M_V = -2$, with a hint for a bending around $M_V = -5$.

In this paper we combine high-resolution simulations of a MW-like halo with a SA galaxy formation model to investigate how various astrophysical processes affect the formation and evolution of satellites around the Milky Way. Our study extends the analysis presented in De Lucia & Helmi (2008), which focused on the formation of the MW galaxy and of its stellar halo. We find that by preventing cooling in haloes with $T_{\rm vir} < 10^4$ K (the atomic hydrogen cooling limit) and including the impact of the reionization of the Universe, our model is able to reproduce the latest measurements of the satellite luminosity function by Koposov et al. (2008). We show that the same model reproduces the metallicity distribution function (MDF) of the MW satellites, by including a route to recycle metals produced in newly formed stars through the hot phase. Our model satellites exhibit several scaling relations similar to those followed by the MW satellites, such as the metallicity-luminosity and the luminosity-size relations. The properties of the model satellites resembling the newly discovered ultra-faint SDSS satellites appear to be sensitive to the SN feedback recipe adopted. As we will discuss in the following, our model suggests that the surviving satellites are generally associated with haloes whose present-day peak circular velocity, $V_{\rm max}$, $\gtrsim 10\,\mathrm{km\,s^{-1}}$, total mass exceeded a few $10^6\,\mathrm{M}_\odot$ at $z \sim 10-20$ and which acquired their maximum dark matter mass well above the cooling threshold, after $z \sim 6$.

This paper is organised as follows. Section 2.1 presents the simulations used in this study, and in Section 2.2 we summarise our semi-analytical galaxy formation model, emphasising the new features added to the model presented in De Lucia & Helmi (2008). In Section 3 we present our main results and in Section 4 we discuss the implications of our study. We give our conclusions in Section 5.

2 THE HYBRID MODEL OF GALAXY FORMATION AND EVOLUTION

2.1 ΛCDM Simulations of a MW-like halo

We have used a series of high resolution simulations of a MW-like halo (Stoehr et al. 2002; Stoehr 2006). We note that this is the exact GAnew series used in previous studies by Li & Helmi (2008), De Lucia & Helmi (2008) and Li et al. (2009). We therefore only summarise the basic properties of the simulations here, and refer the reader to those papers for more details. The simulations were carried out with GADGET-2[1] (Springel et al. 2001) adopting a ΛCDM cosmological model, with $\Omega_0 = 0.3, \Omega_\Lambda = 0.7, h = 0.7$, $\sigma_8(z=0) = 0.9$, and Hubble constant H_0=100h km s^{-1} Mpc^{-1}.

[1] The GAnew simulations were in fact carried out using an intermediate version between GADGET and GADGET-2.

The target MW-like halo was simulated at four increasing resolution levels (the mass resolution was increased by a factor 9.33 each time). In the highest resolution simulation (GA3new), there are approximately 10^7 particles with mass $m_p = 2.063 \times 10^5\,\mathrm{M}_\odot\ h^{-1}$ within the virial radius. Each re-simulation produced 108 outputs, equally spaced logarithmically in time between $z = 37.6$ and $z = 2.3$, and nearly linearly spaced from $z = 2.3$ to present.

Merger trees for all self-bound haloes were constructed as described in detail in De Lucia & Helmi (2008). Virialised structures were identified using the standard friends-of-friends (FOF) algorithm and linking all particles separated by less than 0.2 the mean inter-particle separation. The algorithm SUBFIND (Springel et al. 2001) was then applied to each FOF group to find the gravitationally self-bound substructures. Following Navarro et al. (1997), we define R_{200} as the radius of a sphere enclosing a mass, M_{200}, whose average density is 200 times the critical density of the Universe at redshift z, i.e. :

$$M_{200} = \frac{4\pi R_{200}^3}{3} \cdot 200\delta_{crit}(z) = \frac{100H(z)^2 R_{200}^3}{G}.$$

The velocity, V_{200}, is defined as the circular velocity of the halo at R_{200} ($V_{200} = \sqrt{GM_{200}/R_{200}}$). M_{200} is directly measured from the simulations and used to calculate R_{200} and V_{200}. In our models, we approximate the virial properties of dark matter haloes, e.g. virial radius ($R_{\rm vir}$), virial mass ($M_{\rm vir}$) and virial velocity ($V_{\rm vir}$) by R_{200}, M_{200} and V_{200} respectively, unless otherwise explicitly stated.

Following De Lucia & Helmi (2008), we scaled down the original outputs by a factor of 1.42^3 for the mass and 1.42 for the positions and velocities, in order to have a MW-like halo with $V_{200} \sim 150\,\mathrm{km\,s^{-1}}$ (Battaglia et al. 2005; Smith et al. 2007; Xue et al. 2008). After the scaling, the smallest resolved subhaloes (containing 20 particles) have dark matter mass $M_{\rm DM} \sim 2 \times 10^6\,\mathrm{M}_\odot$ in the highest resolution run (GA3new). $M_{\rm DM}$ denotes the total bound mass at $z = 0$ determined by SUBFIND throughout this paper. The present-day virial mass and the virial radius for the MW-like halo are $M_{200} \sim 10^{12}\,\mathrm{M}_\odot$ and $R_{200} = 209$ kpc, respectively.

2.2 Semi-analytic modelling

We use a semi-analytical galaxy formation model to study the baryonic properties of a MW-like galaxy and its satellites. This model has been developed mainly at the Max–Planck–Institut für Astrophysik and we refer to it as the 'Munich model' later in the text. The essential ideas of any semi-analytic model can be traced back to the works by White & Rees (1978) and White & Frenk (1991), and include physical processes such as the cooling of gas, star formation and feedback due to supernova explosions. Over the years, the Munich model has been enriched with new 'ingredients', e.g. the growth of supermassive black holes (Kauffmann & Haehnelt 2000), the inclusion of dark matter substructures (Springel et al. 2001), chemical enrichment (De Lucia et al. 2004) and AGN feedback (Croton et al. 2006). The model we use in this study has been presented in De Lucia & Helmi (2008) and builds upon the model whose results have been made publicly available (De Lucia & Blaizot 2007). In order to reproduce the properties of the MW satellites, we have made a few modifications to the original model. In the following, we refer to the model used by De Lucia & Helmi (2008) as the MW-model and to the fiducial one used in this work as the satellite-model. Here we give a brief summary of the physical processes implemented in our models which are crucial to the properties of the satellites.

2.2.1 Reionization

Following Croton et al. (2006), we make use of the results by Gnedin (2000) who simulated cosmological reionization and quantified the effect of photoionization on the baryon fraction of low-mass haloes. Gnedin found that reionization reduces the baryon content in haloes whose mass are smaller than a particular 'filtering mass' scale, that varies with redshift. The fraction of baryons, f_b^{halo}, in a halo of mass $M_{\rm vir}$ at redshift z, is decreased compared to the universal baryon fraction[2] according to the ratio of the halo mass and the 'filtering mass', M_F:

$$f_b^{halo}(z,\ M_{\rm vir}) = \frac{f_b}{[1 + 0.26M_F(z)/M_{\rm vir}]^3}. \quad (1)$$

For $M_F(z)$, we use the analytical fitting function given in Appendix B of Kravtsov et al. (2004).

In our fiducial satellite-model, we assume that reionization starts at redshift $z_0 = 15$ and ends at $z_r = 11.5$, while the original MW-model adopted $z_0 = 8$ and $z_r = 7$ (in both models reionization lasts for about 0.12 Gyr). For simplicity, we refer to the reionization epoch, $z_{\rm reio}$, as z_0 hereafter. Our choice of fixing $z_{\rm reio} = 15$ gives the right shape and the normalisation for the satellite luminosity function. We discuss the dependence of the satellites luminosity function on different assumptions for the reionization epoch in Section 3.1.

2.2.2 Cooling

In our model, the cooling of the shock-heated gas is treated as a classical cooling flow (e.g. White & Frenk 1991), with the cooling rate depending on the temperature and metallicity of the hot gas. As in De Lucia et al. (2004), we model these dependences using the collisional ionisation cooling curves of Sutherland & Dopita (1993). For primordial (or low-metallicity) composition, the cooling is dominated by bremsstrahlung (free-free) emission at high temperatures ($T \gtrsim 10^6\,\mathrm{K}$) and it is most efficient at $T \sim 10^5\,\mathrm{K}$ and $\sim 1.5 \times 10^4\,\mathrm{K}$ (the H and He^+ peaks of the cooling function). Line cooling from heavy elements dominates in the 10^6–10^7 K regime for non primordial compositions. For $T < 10^4\,\mathrm{K}$, i.e. below the atomic hydrogen cooling limit, the dominant coolant is molecular hydrogen (H_2). The virial temperature of a halo can be expressed as a function of its virial velocity as:

$$T_{\rm vir}(z) = 35.9 \left(\frac{V_{\rm vir}(z)}{\mathrm{km\,s^{-1}}} \right)^2. \quad (2)$$

Therefore, a halo with $T_{\rm vir} = 10^4\,\mathrm{K}$ corresponds to a virial velocity of $V_{\rm vir} = 16.7\,\mathrm{km\,s^{-1}}$, which is equivalent to $M_{\rm vir} \sim 3 \times 10^7\,\mathrm{M}_\odot$ when $z = 15$, and $M_{\rm vir} \sim 2 \times 10^9\,\mathrm{M}_\odot$ when $z = 0$.

In the MW-model, haloes with $T_{\rm vir}$ lower than $10^4\,\mathrm{K}$, are able to cool as much gas as a $10^4\,\mathrm{K}$ halo with the same metallicity. In the satellite-model, we forbid cooling in small haloes with $T_{\rm vir} < 10^4\,\mathrm{K}$, for any metallicities and at all times. This is a reasonable approximation since molecular hydrogen is very sensitive to photo-dissociation caused by UV photons from (first)

[2] We use the *WMAP* 3-year value $f_b = 0.17$ (Spergel et al. 2007).

stellar objects (Haiman et al. 2000, see also Kravtsov et al. 2004; Koposov et al. 2009).

2.2.3 Star formation and supernova feedback

The star formation model used in this work is described in detail in De Lucia & Helmi (2008), while we refer to Croton et al. (2006) and De Lucia et al. (2004) for details on the supernova feedback models. Cold gas is assumed to be distributed in an exponential disk and provides the raw material for star formation, which occurs at a rate:

$$\psi = \alpha_{\rm SF} M_{\rm sf} / t_{\rm dyn}, \quad (3)$$

where $\alpha_{\rm SF}$ is a free parameter which controls the star formation efficiency, $t_{\rm dyn}$ is the disk dynamical time and $M_{\rm sf}$ is the gas mass above a critical density threshold. As in De Lucia & Blaizot (2007) and De Lucia & Helmi (2008), we fix $\alpha_{\rm SF}$ at 0.03, and adopt a Chabrier IMF. The surface density threshold takes a constant value throughout the disk (see De Lucia & Helmi 2008, for details). At each time step, Δt, we calculate the amount of newly formed stars,

$$\Delta M_* = \psi \, \Delta t. \quad (4)$$

Massive stars explode as SNe and inject energy in the surrounding interstellar medium. In our model, we do not consider the delay between star formation and SN energy (and metals) injection, i.e. the lifetime of such stars is assumed to be zero. The energy injection by SNe per solar mass can be expressed as $V_{\rm SN}^2 = \eta_{\rm SN} \cdot E_{\rm SN}$ where $\eta_{\rm SN} = 8.0 \times 10^{-3}\,{\rm M}_\odot^{-1}$ is the number of SNe per unit solar mass expected from a Chabrier IMF[3] and $E_{\rm SN} = 1.0 \times 10^{51}$ erg is the average energy per SN. The energy released by SNe in the same time interval is:

$$\Delta E_{\rm SN} = \epsilon_{\rm halo} \cdot 0.5 V_{\rm SN}^2 \Delta M_*. \quad (5)$$

where $\epsilon_{\rm halo}$ represents the efficiency with which the energy is able to reheat disk gas. We assume that the amount of cold gas reheated by SNe is proportional to the newly formed stars:

$$\Delta M_{\rm reheat} = \epsilon_{\rm disk} \, \Delta M_*. \quad (6)$$

If this gas were added back to the hot phase without changing its specific energy, the total thermal energy would change by:

$$\Delta E_{\rm hot} = 0.5 \Delta M_{\rm reheat} V_{\rm vir}^2. \quad (7)$$

If $\Delta E_{\rm SN} > \Delta E_{\rm hot}$, SN feedback is energetic enough to eject some of the hot gas outside the halo and we assume that:

$$\Delta M_{\rm eject} = \frac{\Delta E_{\rm SN} - \Delta E_{\rm hot}}{0.5 V_{\rm vir}^2} = \left(\epsilon_{\rm halo} \frac{V_{\rm SN}^2}{V_{\rm vir}^2} - \epsilon_{\rm disk} \right) \Delta M_*. \quad (8)$$

The ejected material can be re-incorporated into the hot component associated with the central galaxy as the halo keeps growing by accreting material from the surroundings (De Lucia et al. 2004; Croton et al. 2006). For the two parameters which regulate the feedback, $\epsilon_{\rm halo}$ and $\epsilon_{\rm disk}$, we assume the values 0.35 and 3.5 respectively, following Croton et al. (2006) and De Lucia & Blaizot (2007). This means that for galaxies with $V_{\rm vir} < 200\,{\rm km\,s^{-1}}$, $\Delta M_{\rm eject} > 0$ for $\Delta M_* > 0$.

[3] This is the fraction of stars with mass larger than $\sim 8\,{\rm M}_\odot$ per unit of stellar mass formed. Note that, since we have adopted an instantaneous recycling approximation, it is more appropriate to compare the metallicities of our model galaxies with elements synthesised by Type II supernovae.

An alternative supernova feedback

Since dwarf galaxies have shallow potential wells, their properties are expected to be particularly sensitive to the adopted SN feedback model. To explore this dependency, we have also used an alternative SN feedback recipe in addition to the 'standard' recipe mentioned above. We note that this alternative feedback recipe is equivalent to the *ejection* model described in De Lucia et al. (2004), and we refer to this paper for more details on this particular feedback model. In the *ejection* model, the gas reheated by SNe is computed on the basis of energy conservation arguments and depends on the galaxy mass as:

$$\Delta M_{\rm reheat} = \frac{4}{3} \epsilon \, \frac{V_{\rm SN}^2}{V_{\rm vir}^2} \, \Delta M_*. \quad (9)$$

Our choices of the feedback parameters ($\epsilon = 0.05$ and $V_{\rm SN} \sim 634\,{\rm km\,s^{-1}}$) imply that galaxies with $V_{\rm vir} < 87\,{\rm km\,s^{-1}}$ would have in this model more heated mass per unit of newly formed stellar mass, compared to the standard recipe (Eq. 6). In this model the material reheated by supernova explosions in central galaxies is assumed to leave the halo and to be deposited in an 'ejected' component that can be re-incorporated into the hot gas at later times. The material reheated by SNe explosions in satellite galaxies is assumed to be incorporated directly in the hot component associated with the corresponding central galaxy.

We will discuss later how our results for the baryonic properties of the satellites depend on the adopted feedback scheme.

2.2.4 Metal recycling through the hot phase

At each time step, the masses exchanged among the four phases: $M_{\rm hot}$, $M_{\rm cold}$, M_*, $M_{\rm eject}$, (i.e. hot gas, cold gas, stars and ejecta) are updated as described in Section 4.7 and Fig. 1 in De Lucia et al. (2004). The metallicity in each phase is denoted as Z_x and is defined as the ratio between the mass in metals in each component (M_x^Z) and the corresponding mass (M_x) where the suffix x is hot, cold, star or eject. In the satellite-model, we include a route to recycle metals produced by newly formed stars through the hot phase of a galaxy. The equations given in Section 4.7 of De Lucia et al. (2004) modify as follows:

$$\dot{M}_*^{\rm Z} = +(1-R) \cdot \psi \cdot Z_{\rm cold}$$

$$\begin{aligned} \dot{M}_{\rm hot}^{\rm Z} &= -\dot{M}_{\rm cool} \cdot Z_{\rm hot} + \dot{M}_{\rm back} \cdot Z_{\rm eject} \\ &\quad + \sum_{sat} (\dot{M}_{\rm reheat} \cdot Z_{\rm cold}) + F_{\rm Zhot} \cdot Y \cdot \psi \end{aligned}$$

$$\begin{aligned} \dot{M}_{\rm cold}^{\rm Z} &= +\dot{M}_{\rm cool} \cdot Z_{\rm hot} - (1-R) \cdot \psi \cdot Z_{\rm cold} \\ &\quad + (1 - F_{\rm Zhot}) \cdot Y \cdot \psi - \dot{M}_{\rm reheat} \cdot Z_{\rm cold} \end{aligned}$$

$$\dot{M}_{\rm eject}^{\rm Z} = +\dot{M}_{\rm eject} \cdot Z_{\rm hot} - \dot{M}_{\rm back} \cdot Z_{\rm eject}.$$

A constant yield Y of heavy elements is assumed to be produced per solar mass of gas converted into stars. The gas fraction returned by evolved stars is $R = 0.43$, appropriate for a Chabrier IMF. In the above equations, $\dot{M}_{\rm cool}$ represents the cooling rate; $\dot{M}_{\rm back}$ provides the re-incorporation rate; $\dot{M}_{\rm reheat}$ is the reheating rate by SNe, and $\dot{M}_{\rm eject}$ is the rate of mass ejected outside the halo.

For the alternative SN feedback recipe, the reheated gas is assumed to be ejected from the cold phase directly for central galaxies. In this case, the metallicity in the ejecta is updated as

$\dot{M}^{\rm Z}_{\rm eject} = +\dot{M}_{\rm reheat} \cdot Z_{\rm cold} - \dot{M}_{\rm back} \cdot Z_{\rm eject}$.

In the MW-model, all newly produced metals returned to the cold phase immediately, i.e. $F_{\rm Zhot} = 0$. Hydrodynamical simulations by Mac Low & Ferrara (1999) suggest that metals can be blown out from small galaxies with gas mass below $10^7\,{\rm M}_\odot$ (corresponding to a halo of $M_{\rm vir} = 3.5 \times 10^8\,{\rm M}_\odot$). In our satellite model, we assume a simple two-state value for $F_{\rm Zhot}$ to account for the above mass dependence:

$$F_{\rm Zhot} = \begin{cases} 0.0 & \text{if } M_{\rm vir} \geqslant 5 \times 10^{10}\,{\rm M}_\odot \\ 0.95 & \text{otherwise.} \end{cases}$$

This means that for galaxies with a dark matter halo with virial mass less than $5 \times 10^{10}\,{\rm M}_\odot$, 95 per cent of newly produced metals are deposited directly into the hot phase in this model.

2.3 Treatment of satellite galaxies

We follow the convention established along the development of the Munich model to classify galaxies according to their association with a distinct dark matter substructure. The galaxy associated with the most massive subhalo in a FOF group is referred to as 'Type 0' or central galaxy. Other galaxies in a FOF group are usually referred to as satellites and are further differentiated into 'Type 1' galaxies, if their dark matter subhalo is still identified, and 'Type 2', when their subhalo has fallen below the resolution limit of the simulation.

When a galaxy becomes a satellite, the dark matter mass of the parent subhalo is approximated using the number of bound dark matter particles given by SUBFIND. The disk size is fixed at the value it had just before accretion. In our model, only Type 0 central galaxies are allowed to accrete the material that cools from the hot gas associated with the parent FOF group. Satellite galaxies do not have hot and ejected components and the cooling is forbidden, i.e. $M_{\rm hot} = M_{\rm eject} = \dot{M}_{\rm cool} = 0$. When a galaxy becomes a satellite, its hot and ejected components are transferred to the corresponding components of the central galaxy. As a consequence, once matter leaves the cold phase of a satellite, it does not rejoin the (Type 1 or Type 2) satellite at a later time, but it can be accreted onto the corresponding central galaxy.

2.4 Model improvements and the central MW-like galaxy

The values of the parameters that enter in the SA model were chosen so as to reproduce several observations of galaxies in the local Universe, in particular the local galaxy luminosity function and the mass and luminosity of MW-like galaxies (see De Lucia et al. 2004; Croton et al. 2006; De Lucia & Blaizot 2007). It is therefore not entirely surprising that this same parameter set provides results that are in nice agreement with observational properties of our MW galaxy (De Lucia & Helmi 2008). In order to obtain a good agreement with the observed properties of the MW satellites, however, we found that we had to implement some slight modifications.

In our satellite-model, we adopt the same parameter set used in De Lucia & Helmi (2008) except for the reionization epoch, $z_{\rm reio}$, and fraction of metal ejected into the hot component, $F_{\rm Zhot}$. Table 1 introduces the SA models that we employ in this study. In the MW-model by De Lucia & Helmi (2008), reionization occurs at $z_{\rm reio} = 8$, haloes with $T_{\rm vir} < 10^4$ K are allowed to cool at the same rate of a 10^4 K halo with the same hot gas metallicity, a 'standard' SN feedback recipe is adopted and all new metals are kept in the cold gas phase ($F_{\rm Zhot} = 0$). Our fiducial model for the satellite galaxies corresponds to the 'satellite-model' (the fourth row in Table 1). In this model, reionization starts at $z = 15$, and 95 per cent of the new metals are deposited directly into the hot component in galaxies with $M_{\rm vir} < 5 \times 10^{10}\,{\rm M}_\odot$. In all models with the prefix 'satellite', we forbid cooling in haloes with $T_{\rm vir} < 10^4$ K.

Below, we briefly discuss the dependence of model results for the central MW-like galaxy on our changes for $z_{\rm reio}$, the cooling in small haloes and metal recycling through hot phase. The results for the satellite galaxies are presented in Section 3. Table 2 summarises the properties of the MW-like galaxies in different SA models at $z = 0$.

The results corresponding to the MW-model are given in the first row (see also Fig. 2 of De Lucia & Helmi 2008). The only difference between the MW-model and the satellite-model A is the suppression of cooling in small haloes. Comparing the results of these two models, we find no significant changes in the properties of the present-day MW-like galaxy. In satellite-model B, we also change $z_{\rm reio}$ to 15 and keep $F_{\rm Zhot} = 0$. The only significant effect of an early reionization is to bring down the black hole mass by ~ 15 per cent compared to the value obtained in the MW-model. The early reionization also results in a slight increase of the stellar mass but this is still well within the observational uncertainties ($M_* \sim 5 - 8 \times 10^{10}\,{\rm M}_\odot$).

Our fiducial satellite-model gives a total stellar mass similar to that obtained from the MW-model and in agreement with current observational constraints. The results of these two models are also very close in terms of the mass of the bulge and the cold gas content. The black hole mass $M_{\rm BH} = 6.9 \times 10^6\,{\rm M}_\odot$ from the satellite-model is in marginal agreement with the latest measurement of the MW black hole mass $M_{\rm BH} = (4.5 \pm 0.4) \times 10^6\,{\rm M}_\odot$ (Ghez et al. 2008). The ejection of metals into the hot component in small galaxies (cf. satellite-model B) only makes the bulge slightly more metal-poor (~ 0.06 dex). Results listed in Table 2 show that the modifications discussed above influence only the properties of dwarf galaxies, while preserving the properties of the MW-like galaxies discussed in De Lucia & Helmi (2008).

The 5th row in Tables 1 and 2 corresponds to a model which incorporates the 'alternative' (or *ejection*) SN feedback scheme described in Section 2.2.3. When compared to the 'standard' scheme, the dependency of the amount of reheated gas on $1/V^2_{\rm vir}$ in this scheme results in a more efficient feedback for small galaxies and in a less efficient ejection for more massive systems like the MW galaxy. These galaxies tend to have larger stellar masses, a more massive bulge and tend to be more metal-rich in this scheme. As we will show in Section 3, however, this alternative feedback scheme is able to better match the properties of the MW satellites.

We therefore propose a combination of these two feedback recipes to account for the properties of galaxies on large and small mass scales. This model corresponds to the 'satellite-model *combined*', and in this scheme, we calculate the amount of gas reheated by SNe depending on the local potential well (mass of the associated subhalo):

$$M_{\rm reheat} = \begin{cases} \frac{4}{3}\epsilon\,\frac{V^2_{\rm SN}}{V^2_{\rm vir}}\,\Delta M_* & \text{if } V^2_{\rm vir} < \frac{4}{3}\frac{\epsilon}{\epsilon_{\rm disk}}\,V^2_{\rm SN} \\ \epsilon_{\rm disk}\Delta M_* & \text{otherwise.} \end{cases}$$

The reheated gas is treated as in the *ejection* scenario, i.e. it is added to the ejected component of a central galaxy and lost into the hot component for a satellite. The 'satellite-model *combined*' entry in Table 2 lists the properties of the MW-like galaxy in this scheme. As expected, the stellar mass, the total and bulge metallicity, as well as the total luminosity are now very similar to what we get with the

Table 1. Nomenclature and features of the semi-analytic models used in this study.

Model Name (1)	z_0, z_r (2)	cooling for $V_{\rm vir} < 16.7\,{\rm km\,s^{-1}}$ (3)	SN feedback (4)	$F_{\rm Zhot}$ (5)
MW-model	(8, 7)	Yes	Standard	0.0
satellite-model A	(8, 7)	No	Standard	0.0
satellite-model B	(15, 11.5)	No	Standard	0.0
satellite-model	(15, 11.5)	No	Standard	(0.95, 0.0)
satellite-model *ejection*	(15, 11.5)	No	ejection	(0.95, 0.0)
satellite-model *combined*	(15, 11.5)	No	combined	(0.95, 0.0)

Different columns list: (1) the model name; (2) the reionization epoch; (3) the adopted cooling recipe in haloes with $T_{\rm vir} < 10^4$ K; (4) the adopted feedback recipe; (5) the fraction of metals injected directly into the hot component.

Table 2. Properties of the Milky Way-like galaxy in the semi-analytic models employed in this study, for the GA3new simulation.

Model Name (1)	M_* [$10^{10}\,{\rm M_\odot}$] (2)	$M_{\rm bulge}$ [$10^{10}\,{\rm M_\odot}$] (3)	$M_{\rm coldgas}$ [$10^{10}\,{\rm M_\odot}$] (4)	$M_{\rm BH}$ [$10^{6}\,{\rm M_\odot}$] (5)	Log$\frac{Z_*}{Z_\odot}$ [dex] (6)	Log$\frac{Z_b}{Z_\odot}$ [dex] (7)	M_B [mag] (8)
MW-model	5.73	0.64	1.06	8.2	-0.05	-0.28	-19.53
satellite-model A	5.75	0.64	1.07	8.0	-0.05	-0.28	-19.50
satellite-model B	5.85	0.62	1.11	7.1	-0.06	-0.30	-19.52
satellite-model	5.88	0.63	1.11	6.9	-0.06	-0.35	-19.52
satellite-model *ejection*	8.26	2.58	1.09	12.8	0.12	0.00	-19.08
satellite-model *combined*	5.02	0.84	0.95	12.0	-0.08	-0.25	-19.53

Different columns list: (1) the model name; (2) stellar mass; (3) mass of the bulge; (4) cold gas content; (5) mass of the black hole; (6) logarithmic value of the total stellar metallicity; (7) logarithmic value of the bulge metallicity; (8) B-band absolute magnitude corrected for internal dust attenuation.

standard feedback scheme, albeit the bulge (and the black hole) are now more massive. The last two models listed in Table 1 populate the same set of subhaloes with stars, with almost identical properties. For simplicity, we will not discuss the results of the *combined* scheme for satellite galaxies.

3 THE MILKY WAY SATELLITES

In this Section, we define as SA model satellites of the MW-like galaxy those that satisfy the following conditions at $z = 0$: (i) a satellite has to belong to the same FOF group where the MW-like galaxy is; (ii) the distance to the MW-like galaxy must be < 280 kpc; (iii) the galaxy is associated with a dark matter subhalo (i.e. it has to be Type 1 galaxies). The distance cut corresponds to the current observational limits, but we include in our comparison the very distant and recently discovered satellite Leo T (at ~ 420 kpc from the Milky Way).

We do not consider here satellites that had their dark matter haloes tidally stripped below the resolution limit of the simulation (Type 2 galaxies). This selection is motivated by the fact that while resolved, our Type 1 galaxies are dark matter dominated at all radii (see Section 3.5, and in agreement with observations of satellites around the MW and M31, e.g. Simon & Geha 2007; Strigari et al. 2007, 2008; Walker et al. 2009). Since Type 2 galaxies in our fiducial model, reach a maximum virial mass during their evolution larger than $6.8 \times 10^7\,{\rm M_\odot}$, this means that these galaxies have lost more than 97 per cent of their dark matter by present. Therefore it is quite unlikely that a bound stellar core would survive such a severe tidal stripping. We will discuss more about Type 2 model galaxies in Section 4.2. Throughout this paper, we will refer to subhaloes that host stars as 'luminous satellites' or simply 'satellites', and will refer to those that do not host any star as dark satellites or subhaloes.

3.1 The satellite luminosity function

Our fiducial satellite-model gives 51 luminous satellites within 280 kpc for GA3new. This is in good agreement with the estimated 'all sky' number of satellites (~ 45) brighter than $M_V = -5.0$ by Koposov et al. (2008). If we remove the distance constraint, the number of satellites is only increased by one, and the number of subhalos varies from 1865 to 1869.

The mass functions for the fiducial satellite-model and of the surviving subhaloes within 280 kpc in GA3new are shown in Fig. 1. The mass plotted here is the dark matter mass at $z = 0$ determined by SUBFIND. As indicated by the dashed histogram, all subhaloes with present-day $M_{\rm DM} > 10^9\,{\rm M_\odot}$ resolved in GA3new host luminous satellites. The mass function of these subhaloes deviates from the power-law shape mass function of the full subhalo population and is fairly flat below $M_{\rm DM} = 10^9\,{\rm M_\odot}$, down to the resolution limit ($M_{\rm DM} \sim 10^{6.5}\,{\rm M_\odot}$). For comparison, the dotted histogram in Fig. 1 shows the mass function of surviving subhaloes, within the same distance range from the central galaxy, from the lower reso-

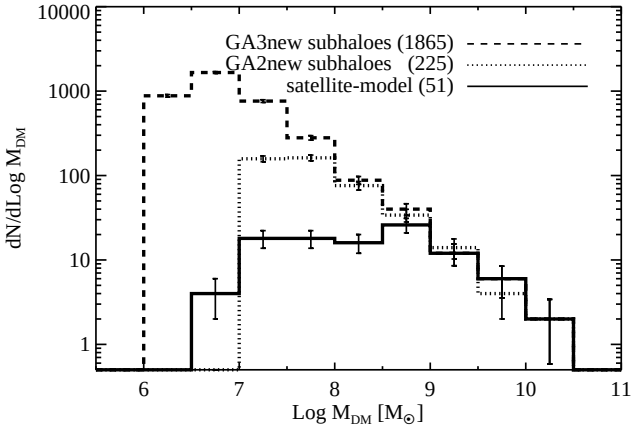

Figure 1. The solid histogram shows the present-day mass function of model satellites using the satellite-model for the highest resolution simulation. Error bars denote the 1-σ Poisson uncertainties. The dashed histogram shows the subhalo mass function for the highest resolution simulation, which steeply rises up to the resolution limit. The dotted histogram is the subhalo mass function for a lower resolution simulation (i.e. GA2new).

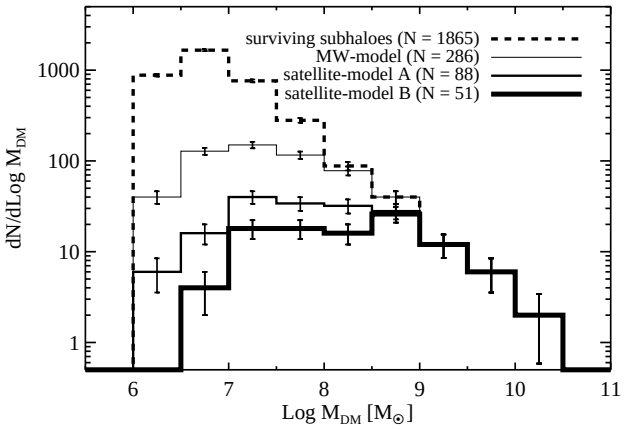

Figure 2. Present-day mass functions (solid histograms) for dark matter subhaloes associated with satellites predicted by the semi-analytic models listed in Table 1. The dashed histogram again indicates the subhalo mass function for the GA3new simulation.

Table 3. Number of satellites around the model MW galaxy for the different SA models used in this study for the GA3new simulation.

Model Name (1)	$N_{\rm sat}$ (2)	z_0, z_r (3)	$F_{\rm Zhot}$ (4)
MW-model	286	(8, 7)	0.0
satellite-model A	88	(8, 7)	0.0
satellite-model B	51	(15, 11.5)	0.0
satellite-model	51	(15, 11.5)	(0.95, 0.0)
satellite-model *ejection*	51	(15, 11.5)	(0.95, 0.0)
satellite-model *combined*	51	(15, 11.5)	(0.95, 0.0)

Different columns list: (1) the model name; (2) the number of luminous satellites; (3) the adopted reionization epoch; (4) the fraction of metals ejected directly into the hot component.

lution simulation GA2new. The smallest subhalo which could be resolved in GA2new has $M_{\rm DM} \sim 2 \times 10^7\,{\rm M}_\odot$. The subhalo mass functions from the two simulations agree well down to $10^8\,{\rm M}_\odot$. At lower masses, numerical effects start to become important for GA2new. However, the number of satellites with $M_{\rm DM} < 10^9\,{\rm M}_\odot$ is still lower than the number of subhaloes resolved in GA2new, which suggests that numerical resolution should not be an issue and that the observed decline of luminous satellites is a result of how we model the baryonic physics, e.g. SN feedback, as we will see later.

Fig. 2 compares the mass function for the SA models explored in this study. In Table 3, we list the number of luminous satellites for these models. Note that all the models which adopt $z_{\rm reio} = 15$ and forbid cooling in haloes with $V_{\rm vir} < 16.7\,{\rm km\,s^{-1}}$, i.e. satellite-model B, satellite-model, satellite-model *ejection* and satellite-model *combined*, populate galaxies in the same set of 51 subhaloes. The mass functions of these four models are therefore identical.

Fig. 3 shows the luminosity functions of the first three SA models listed in the tables. The (red) dashed line shows the 'all sky SDSS' power-law luminosity function of satellites within 280 kpc, estimated by Koposov et al. (2008). For satellite-model B, we show the 1-σ Poisson noise. The filled circles show the luminosity function of the 22 known satellites of the MW, including the latest ultra-faint satellite Leo V (Belokurov et al. 2008). As a reference, in the MW-model the number of surviving satellites is 286. The drastic difference between the MW- and the satellite-model B is mostly at the faint end of the luminosity function, and it is due to the combined effect of an early reionization and no cooling in small haloes. In a model with no cooling in small haloes and a later reionization, the number of satellites is 88 (compare the MW-model and the satellite-model A). The number of satellites is further reduced to 51 when assuming an earlier reionization epoch ($z_{\rm reio} = 15$), with a reduction of galaxies in the luminosity range $M_V \in [-7, -10]$ compared to a model with a later reionization. We have also experimented values for $z_{\rm reio}$ at redshift 10 and 12 and found a number of surviving satellites of $N_{\rm sat} = 79$ and 58, respectively. To summarise, these choices of $z_{\rm reio} = [8, 10, 12, 15]$ all give a number of satellites down to $M_V = -5$ which is consistent with the estimation by Tollerud et al. (2008) (see their Fig. 6). However, after examining the shape of the luminosity functions with different $z_{\rm reio}$, we decided to use $z_{\rm reio} = 15$ in our fiducial model, as this choice gives both the right normalisation and a shape which is in better agreement with the observational measurements (see next paragraphs). We recall that our results are based on only one halo, with mass comparable to that estimated for our Milky Way. A certain scatter in model predictions, due e.g. to the assembly history of the parent halo, is expected and this might be significantly larger than the Poisson noise plotted in Fig. 3.

The left panel in Fig. 4 shows the luminosity function of the satellites in our fiducial satellite-model (solid histograms), compared to the 'all sky SDSS' luminosity function by Koposov et al. (2008) and the observational data for the 22 known MW satellites. The model luminosity function covers a similar luminosity range as the 22 MW satellites though the model predicts a lower number of faint ($M_V > -5$) satellites with respect to the expected 'all sky' luminosity function. In fact, the satellite-model does not predict any satellite fainter than $M_V = -4$ mag. On the other hand, it shows an excess with respect to the data of $10 - 15$ satellites around $M_V = -10$. These satellites in excess are all within a dis-

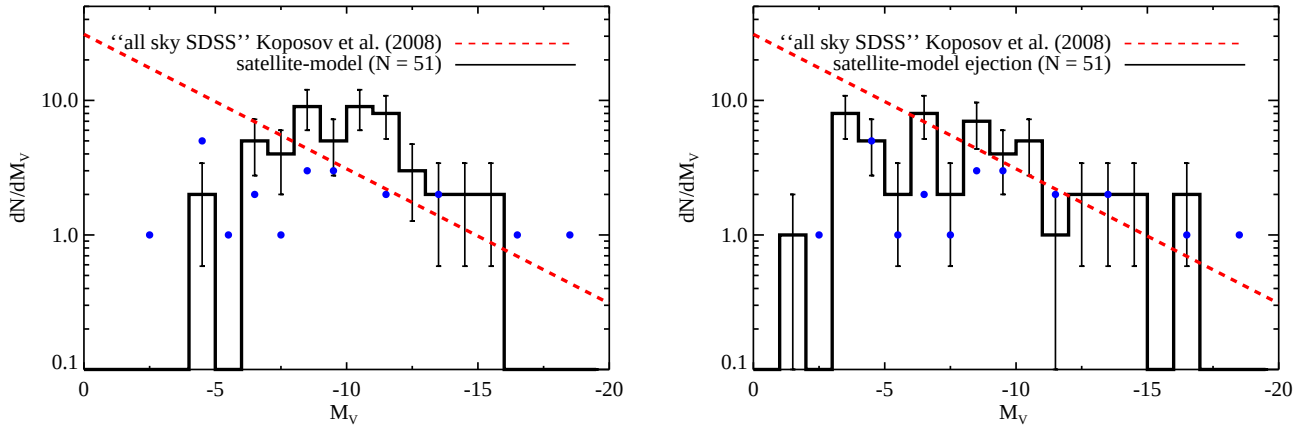

Figure 4. Luminosity function for the observed MW satellites (filled circles and red dashed line) and for the model satellites (black histograms). The left panel is for our fiducial model and the right panel is for the model with a more efficient SN feedback for small galaxies (see Section 2.2.3). Data are the same as those in Fig. 3.

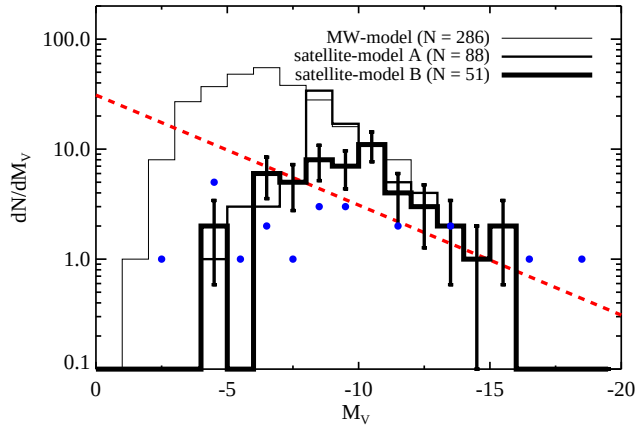

Figure 3. Luminosity function of the observed MW satellites and for the model satellites around a MW-like galaxy, for the first three models listed in Table 3. The integrated V-band luminosities of MW satellites (dots) are taken from various sources. The classical dSphs are from Mateo (1998); most of the ultra-faint dwarfs are from Martin et al. (2008), except Leo T (Ryan-Weber et al. 2008) and Leo V (Belokurov et al. 2008).

tance of 200 kpc from the host galaxy and have half-light radii between 100 and 500 pc. They should therefore have appeared in the 'all-sky' SDSS luminosity function if they existed (provided the distribution for these bright satellites is isotropic, as assumed by Koposov et al. 2008). It also seems that the model under-predicts the number of very bright satellites. This is, however, the regime where both the data and the simulations suffer from small number statistics.

A comparison to Fig. 3 shows that the luminosity function given by satellite-model B and by satellite-model are very similar, implying that satellite luminosities do not depend strongly on the fraction of newly produced metals put into the hot component of a galaxy. However, the metallicity distribution functions differ significantly (see Section 3.2).

The right panel of Fig. 4 shows the luminosity function of surviving satellites resulting from the alternative feedback scheme (satellite model *ejection*). This model luminosity function agrees very well with the observations. When compared with that from the standard feedback scheme, the alternative luminosity function extends to fainter luminosities, reaching $M_V \sim -3$ and does not show any excess at $M_V \sim -10$. Note that in the satellite-model *ejection*, the same 51 subhaloes are populated with luminous galaxies. This suggests that the SN feedback alone is unlikely to solve the 'missing satellites problem' (Somerville 2002), and that the presence/absence of a luminous galaxy within a dark matter substructure is due to the particular assembly and dynamical history of the halo, and to the reionization history of the Universe.

These different results are entirely due to the SN scheme adopted. In the *ejection* scheme, the amount of gas reheated by SNe scales as $1/V_{\rm vir}^2$, and for a galaxy with $V_{\rm vir} < 87\,{\rm km\,s^{-1}}$, more gas is heated by per unit of newly formed stars with respect to the standard scheme, where the amount of gas heated by SNe is only proportional to the amount of newly formed stars. In this latter case, for galaxies with low star formation rates (as is the case for galaxies that live in small subhaloes), only very little gas is heated. As long as the density threshold for star formation is met, these galaxies keep forming stars. This is most likely the reason why our fiducial model exhibits an excess of satellites around $M_V \sim -10$ and a lack of ultra faint objects in the luminosity function. In the alternative feedback model, when star formation occurs in a central galaxy, some cold gas is ejected outside the halo, and has to wait several dynamical time-scales to be reincorporated into the hot halo, delaying any subsequent star formation. Furthermore, the impact on the star formation of a satellite galaxy associated with a subhalo with $V_{\rm vir} < 87\,{\rm km\,s^{-1}}$ is more drastic in this model, because the ejected gas cannot be re-incorporated onto the satellite any longer. Small satellites therefore consume their cold gas reservoir more efficiently in this *ejection* scenario, which causes the surface densities of the cold gas to fall below the criterion for forming stars.

Given the reasonable match of the satellite-model and of satellite-model *ejection* to the observed luminosity functions, in the rest of the paper we will concentrate on the properties of the satellite populations in these two SA models.

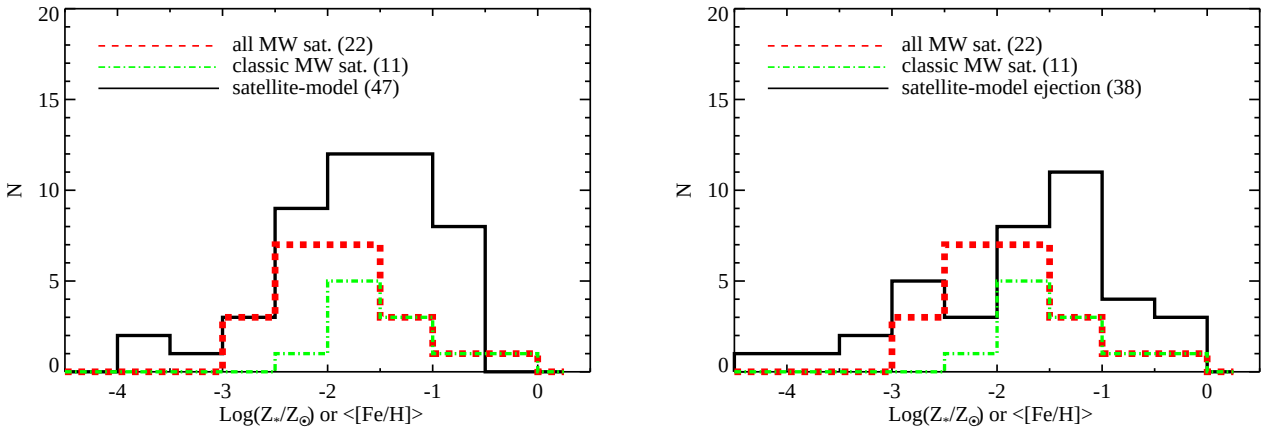

Figure 5. Histogram of the mean iron abundance $[\mathrm{Fe/H}]$ determined for red giant branch stars in the MW satellites. For the model satellites we plot $\log(Z_*/\,\mathrm{Z}_\odot)$. The left panel compares the MW satellites with model satellites from our fiducial model and the right panel from the model with a more efficient SN feedback for dwarf galaxies (see Section 2.2.3). Data for the MW satellites are taken from various sources: LMC and SMC from Westerlund (1997); Sgr from Cole (2001); Ursa Minor and Draco from Harbeck et al. (2001); Sextans, Sculptors, Carina and Fornax from the DART survey (Helmi et al. 2006); Leo II from Koch et al. (2007); Leo I from Koch et al. (2007). For the newly discovered SDSS ultra-faint dwarfs, we take the measurements from Kirby et al. (2008), except for Böotes I for which we use Muñoz et al. (2006), Böotes II from Koch et al. (2009) and Leo V from Walker et al. (2009).

3.2 The metallicity distribution

The left panel of Fig. 5 compares the metallicity distribution of model satellites in our fiducial satellite-model with the observed distribution. The metallicity in our model is mass-weighted and is defined as the ratio between the mass of metals in stars and total stellar mass:

$$Z_* = M_*^{\mathrm{Z}}/M_*.$$

Since our model does not distinguish the long-lived main iron contributors (SN Ia) from the short-lived α-elements enrichers (SN II), a direct comparison of Z to $[\mathrm{Fe/H}]$ is questionable. Nevertheless, here we assume that the logarithmic value of the mass-weighted metallicity normalised to the solar value ($\mathrm{Z}_\odot = 0.02$) can be compared qualitatively with the $[\mathrm{Fe/H}]$ derived from spectra of Red Giant Branch stars in the MW satellites.

Among the 51 surviving satellites in the satellite-model, four of them are free of metals since they have only made stars once from pristine gas. These four metal-free satellites all have present-day $M_{\mathrm{DM}} \lesssim 10^9\,\mathrm{M}_\odot$ and M_* of $10^4 - 10^5\,\mathrm{M}_\odot$. We do not include these 'metal-free' satellites in the left panel of Fig. 5 and (metallicity) related discussions. Fig. 5 shows the histograms of the mean $[\mathrm{Fe/H}]$ of resolved stars in each MW satellite. The distribution of the 11 classical MW satellites is shown by the dotted-dashed histogram, while the corresponding distribution including also 11 ultra-faint satellites is given by the dashed histogram. The metallicity distributions of model and MW satellites cover similar ranges. However, the peak of the metallicity distribution for the 22 MW satellites is shifted to lower values with respect to the corresponding distribution from the satellite-model. The excess of model satellites in the range of $-2 < \log(Z_*/\,\mathrm{Z}_\odot) < -0.5$ corresponds to the bump at $M_V \simeq -10$ seen in the luminosity function.

If we had set $F_{\mathrm{Zhot}} = 0$ (as in satellite-model B), the predicted metallicity distribution would be shifted towards even higher metallicity. In this case, 36 satellites are more metal-rich than $\log(Z_*/\,\mathrm{Z}_\odot) = -1$, and only 11 of them have $\log(Z_*/\,\mathrm{Z}_\odot) < -1$, inconsistent with the observations. This is why our fiducial model is preferred to satellite-model B.

In the right panel of Fig. 5 we plot the metallicity function of the 38 non metal-free[4] satellites in the satellite-model *ejection*. The peak of this distribution is also shifted to slightly higher values than observed, but it has a more even distribution compared to the standard recipe. As discussed in Section 3.1, this is due to the fact that satellites with $V_{\mathrm{vir}} < 87\,\mathrm{km\,s^{-1}}$ loose more of their cold gas reservoir (and a larger fraction of their metals, see Section 2.2.4) in this model with respect to the standard feedback scheme.

3.3 Star formation histories

In Fig. 6 we present the evolution of the stellar mass and the SUBFIND dark matter mass predicted in our fiducial satellite-model. We remind that this model does not give any satellite fainter than $M_V = -4$, and gives only 2 satellites fainter than $M_V = -5$. We therefore restrict our comparisons to the classical MW satellites, and we sort them by their present-day luminosity into three bins: luminous ($-16 < M_V < -13$, similar to Sagittarius and Fornax), intermediate ($-12 < M_V < -10$ like Leo I and Sculptor), and faint ($-10 < M_V < -8$ i.e. Leo II, Sextans, Carina, UMi and Draco). Satellites belonging to these three bins are shown from top to bottom in Fig. 6. We do not include here the two model satellites (one in the luminous and one in the intermediate luminosity bin) which have more stellar mass than dark matter mass at $z = 0$, due to significant tidal interactions with the main halo. We recall that in our modelling, we do not account for tidal stripping of stars and for the loss of the cold gas due to e.g. ram-pressure. Therefore, we also refrain from considering systems which form > 50 per cent of their stars after becoming satellites of the MW-like halo. This choice is motivated by the prevalence of old stars (i.e. > 10 Gyr) seen in the MW dSphs (Dolphin et al. 2005; Orban et al. 2008). When excluding these galaxies, the number of satellites is reduced from 16 to 13 in the intermediate bin; 14 to 7 in the low luminosity bin. We will later see that faint satellites are mostly accreted before $z = 1$ thus their gas should have been reduced due to the interactions with

[4] i.e. 13 satellites are 'metal-free' in this case.

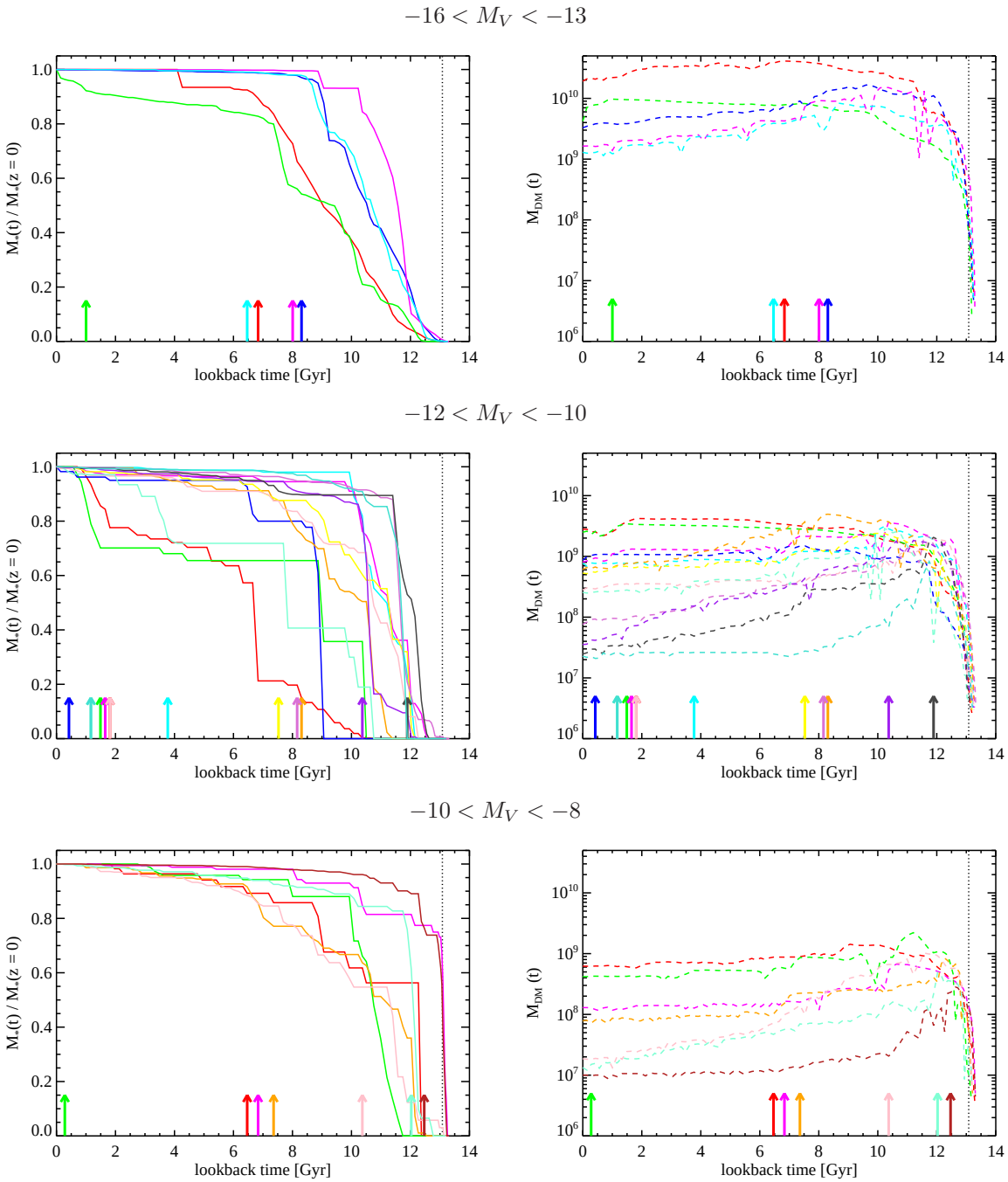

Figure 6. Evolution of the stellar mass (left) and dark matter mass (right) for satellites in the fiducial satellite-model. Satellites are sorted by $M_V(z=0)$ into three groups: $-16 < M_V < -13$ (top panel); $-12 < M_V < -10$ (middle panel); $-10 < M_V < -8$ (bottom panel). Stellar masses are normalised by the present-day values, $M_*(z=0)$. Different colours correspond to different satellites, and the arrows indicate the accretion time, defined as when a satellite was identified as a central galaxy for the last time. The same colour is used to plot the stellar and the dark matter mass for a given satellite in the panel aside. The vertical dashed lines mark the end of the reionization, $z_r = 11.5$, in the satellite-model.

the central galaxy and the star formation should have (on average) ceased shortly after being accreted.

It is encouraging that the model satellites show in Fig. 6 all contain stars older than 10 Gyr regardless of their luminosities, in good agreement with observations[5]. The most luminous satellites build up their stellar content over a longer period of time compared to the faintest ones as observed in the Local Group satellites (Dolphin et al. 2005). The five systems that have been accreted earliest (> 9 Gyr), are associated with fainter satellites ($M_V > -12$), and are dominated by old stars, which means that these galaxies

[5] In the full sample of model satellites, 43 out of 51 made their first generation of stars $\gtrsim 10$ Gyr ago. Those that are not dominated by old stellar populations are excluded in the analysis here with the criterion that half of the stars were in place before the accretion.

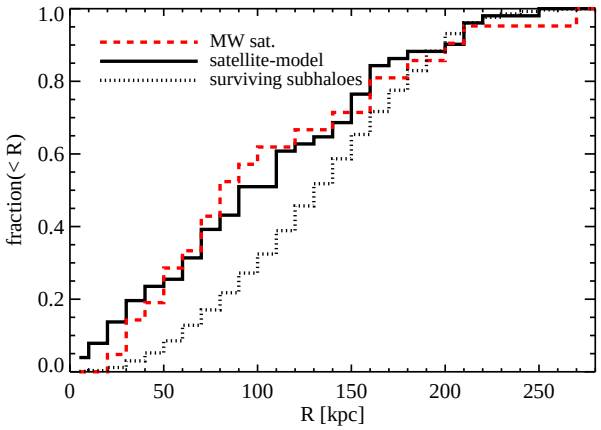

Figure 7. Normalised cumulative radial distributions of the MW satellites (dashed line) compared with that for model satellites (solid line) and for the dark matter subhaloes (dotted line) at $z = 0$. The distance from the Sun to the Galactic centre is taken as $\mathrm{R}_\odot = 8.0$ kpc.

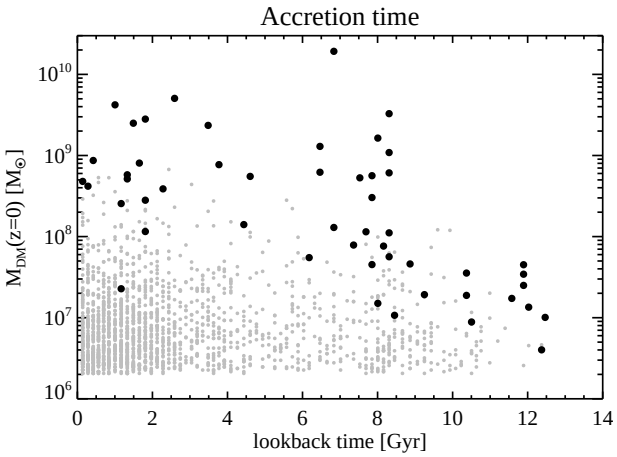

Figure 8. Present-day bound dark matter mass as a function of the accretion time. Black symbols represent the luminous model satellites, while grey symbols mark dark matter subhaloes which failed to form stars.

stopped forming stars soon after the accretion. The most luminous model satellites are associated with massive dark matter subhaloes ($M_{\rm DM} > 10^9\,\mathrm{M}_\odot$) at present time. The Figure also shows that all bright satellites consist of less than 1 per cent of stars made by the end of the reionization ($z = 11.5$ equivalent to a lookback time of ~ 13 Gyr), while a few of the faint ones contain > 50 per cent of such very old stars. None of the most luminous satellites was accreted before $z \sim 1$, and they have the most extended star formation histories and reside in the most massive haloes. This is a natural consequence of the fact that subhaloes that were accreted early, have typically experienced a more significant mass loss than those accreted later (De Lucia et al. 2004; Gao et al. 2004). As explained earlier, no cooling is allowed on satellite galaxies in our model. After accretion, these galaxies keep forming stars, with the size of their gaseous disk fixed at the value when they were accreted. The surface density of the gas soon drops below the density threshold for star formation, therefore rapidly quenching any further star formation in these galaxies.

3.4 Other properties of the satellites

3.4.1 Radial distribution

Fig. 7 shows the cumulative radial distribution of the MW satellites as a dashed line, and of the model satellites as a solid line. Here we only compare our model results with satellites observed within a galactocentric distance of 280 kpc (i.e. excluding Leo T). The median distances of the two distributions agree well. For comparison, we also show the distribution of all surviving dark matter subhaloes (with or without stars) as a dotted line. It is clear that the radial distribution of subhaloes is much less concentrated compared to that of the MW and the model satellites. The reason why our model satellites show a cumulative radial distribution similar to that of the MW satellites can be understood from Fig. 8. This Figure shows the present-day $M_{\rm DM}$ as a function of the accretion time. The small grey circles are for the 'dark' satellites, and the larger black symbols are for those subhaloes which host luminous satellites. The bulk of dark satellites (i.e. subhaloes without stars) in the mass range of $10^6\,\mathrm{M}_\odot < \mathrm{M_{DM}} < 10^7\,\mathrm{M}_\odot$ have been accreted in the last two Gyr, and are preferentially found in the outskirts of the MW halo as, for this mass scale, dynamical friction is not important. Since these small dark satellites dominate by number, this leads to a much more even distribution for subhaloes than for the luminous satellites. Half of the satellites were accreted more than 7 Gyr ago, and the most massive ones (e.g. $M_{\rm DM} > 10^9\,\mathrm{M}_\odot$) at $z = 0$ were all accreted after $z \sim 1$ (see also Fig. 6). There is also a clear bias for the least massive subhaloes hosting stars to have been accreted earlier (as mentioned in Section 3.3).

3.4.2 Luminosity-size relation

Here we compare the half-light radii, $r_{1/2}$, of model satellites with the observed distribution as a function of the total V-band absolute magnitude. The left panel in Fig. 9 is for our fiducial model, while the right panel is for the alternative feedback scheme. The size of a satellite in our models is obtained assuming the stars are distributed in an exponential disk and is roughly proportional to the virial radius of the associated dark matter subhalo, i.e. $r_{1/2} \approx 1.2\lambda R_{200}$ [6], where λ is the spin parameter of the associate DM halo. In Fig. 9 we show the classical dSphs and the ultra-faint satellites with asterisks and diamonds respectively. The black circles show model satellites. The half-light radii of the ultra-faint satellites are from the recent study by Martin et al. (2008) based on SDSS data, while those of the classical ones are from van den Bergh (2000).

Model satellites with either of the feedback recipes have sizes between ~ 30 to 2000 pc, in quite good agreement with the MW satellites, especially the classical ones. For the luminous satellites, both models extend to larger sizes. The lack of faint satellites below $M_V = -5$ in the fiducial model makes the comparison with the ultra-faint satellites inconclusive. The compact satellites with $r_{1/2} < 100$ pc are a few magnitudes brighter than the ultra-faint MW satellites of similar size in this model.

If we compare the sizes of galaxies associated with the same DM subhalo in the two feedback schemes, those given by the alternative feedback recipe (right panel) are a bit larger than in the standard feedback model. This is expected as in the alternative feedback scheme, more gas is ejected by SNe in small (central) galaxies and

[6] $r_{1/2} \approx 1.68\,r_D$ for an exponential disk, and r_D is the scale length of the disk which is computed as $r_D \sim \frac{\lambda}{\sqrt{2}} R_{200}$ to the first order.

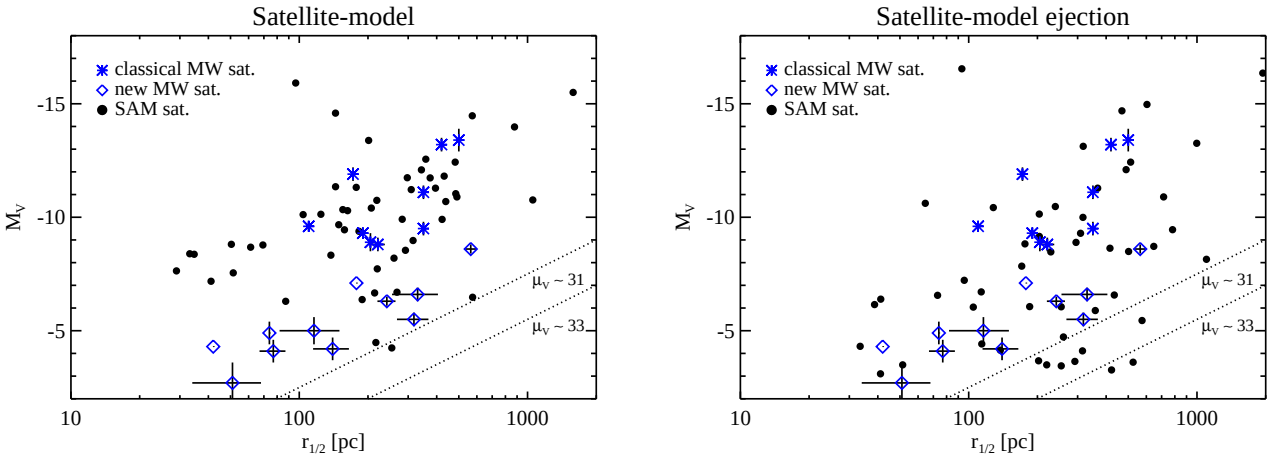

Figure 9. Luminosity as a function of the half-light radius for the MW and model satellites. Observational measurements are taken from various sources: For the classical dSphs, data are from the compilation of van den Bergh (2000). Data for the ultra-faint dwarfs are from Martin et al. (2008), except for Leo V which is taken from Belokurov et al. (2008). See the caption of Fig. 4 for the sources of the total V-band luminosity.

this is reincorporated later, after the halo has grown in mass and size. Since the alternative feedback recipe pushes the luminosity function towards the fainter end, the comparison with the ultra-faint satellites is in better agreement than in the standard recipe. In addition, there are some faint satellites that are larger than the observed ultra-faint systems with central surface brightness fainter than the current observational limit $\mu_v \sim 30\,\mathrm{mag\,arcsec^{-2}}$ (see dotted lines in the Figure).

3.4.3 *Metallicity-luminosity relation*

The classical MW satellites are known to follow a metallicity-luminosity relation with metallicity increasing with increasing luminosity (Mateo 1998). Fig. 10 shows the distribution of model satellites (circles) in the metallicity-luminosity plane, together with the observational measurements for classical (asterisks) and new (diamonds) MW satellites. Black circles are for the fiducial model with the standard feedback scheme, and grey circles are used for the *ejection* model with the alternative feedback scheme. Again, we compare $Z_*/\,\mathrm{Z}_\odot$ for the model satellites with the averaged $[\mathrm{Fe/H}]$ for stars in the MW satellites so care is needed when interpreting these results. The error bars on the $[\mathrm{Fe/H}]$ values indicate the spread of the distributions in each MW satellite rather than measurement uncertainties. The model satellites in the fiducial model follow a similar trend as the classical MW satellites, while it is not possible to compare results from this model to the bulk of ultra-faint satellites since the model does not predict galaxies with luminosity less than $L_V \sim 10^{4.5}\,\mathrm{L}_\odot$ (see also Fig. 4). The excess of model satellites seen in the luminosity function (Fig. 4 left panel) around $M_V \sim -10$ corresponds to objects with $\log(Z_*/\,\mathrm{Z}_\odot)$ in $[-2.0, -1.0]$ dex, and also produces a 'bump' in the metallicity distribution.

With the alternative SN feedback recipe, model satellites also follow the relation of the classical satellites with some hints for metallicities larger than observed for $L_V > 10^6\,\mathrm{L}_\odot$. At the faint luminosity end, there is better agreement with the ultra-faint satellites, since the alternative feedback recipe predicts fainter and metal-poor satellites below $L_V = 10^5\,\mathrm{L}_\odot$. From our model results, it is not clear whether the luminosity-metallicity relation has a lower limit since we are affected by the resolution at the very low mass end. It is also not clear whether the predicted relation deviates from the ultra-faint satellites below $L_V = 10^5\,\mathrm{L}_\odot$. It is interesting to note that if we follow the ridge of the observed luminosity-metallicity relation from the high and metal-rich end down to $L_V = 10^5\,\mathrm{L}_\odot$, the corresponding $[\mathrm{Fe/H}]$ is ~ -2.5 which happens to be the lower limit for the empirical relation to convert the equivalent width of Ca II triplet to $[\mathrm{Fe/H}]$ for RGB stars in dSph galaxies (Battaglia et al. 2008).

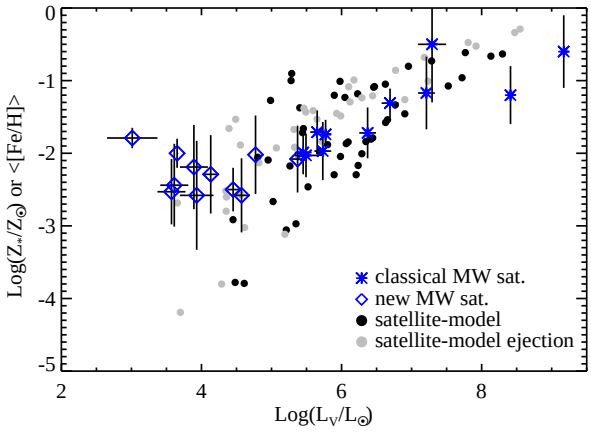

Figure 10. Metallicity-luminosity relation for model and MW satellites. Black circles show model satellites in the fiducial model, and grey circles are used for the *ejection* model. For the model satellites, the logarithmic values of the total metallicity in stars normalised to the solar value ($\mathrm{Z}_\odot = 0.02$) are plotted. For the MW satellites, shown in (blue) asterisks and diamonds, the mean $[\mathrm{Fe/H}]$ is used, and error bars denote the dispersions of $[\mathrm{Fe/H}]$ in each galaxy. See the captions of Fig. 3 and Fig. 5 for the data sources.

3.4.4 *Cold gas content*

The majority of the MW dSph satellites (including the ultra-faint ones, see Grcevich & Putman 2009) are gas deficient. In Fig. 11, we show the cold gas content as a function of the luminosity for our model satellites and compare model results with observational

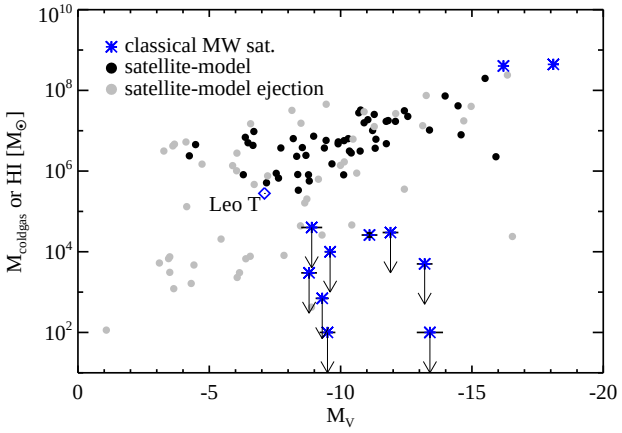

Figure 11. Cold gas content as a function of V-band absolute magnitude. Black circles are used for the standard feedback scheme, and grey circles for the alternative scheme. HI masses are taken from Mateo (1998) for the classical dSphs, and from Brüns et al. (2005) for the Magellanic Clouds. Apart from the gas rich Magellanic Clouds and Sculptor, most of classical dSphs are only constrained with upper limits (indicated by the downward pointing arrows). The distant Leo T is the only one with a clear detection of $M_{\rm H\,I} = 2.6 \times 10^5\,{\rm M}_\odot$ among the newly discovered ultra-faint satellites (Ryan-Weber et al. 2008). The other ultra-faint satellites have no detected HI or an upper limit of $M_{\rm H\,I} \lesssim 10^3\,{\rm M}_\odot$ (Grcevich & Putman 2009) and are not plotted here.

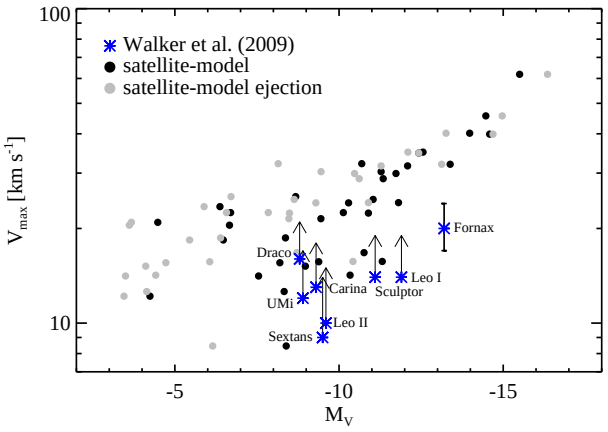

Figure 12. $V_{\rm max}$ as a function of the V-band integrated magnitude for the non tidally disturbed model satellites. Black symbols show predictions for the fiducial model, and grey symbols are used for the *ejection* model. Data for eight classical MW dSphs are taken from Walker et al. (2009). The lower limits on $V_{\rm max}$ are indicated with the upward arrows except for Fornax dSph whose $V_{\rm max}$ is better constrained.

measurements. The Figure shows that model satellites (from either feedback model) are much more gas-rich than the observed counterparts, by factors of a few hundred, except at the brightest end. The satellites from the alternative feedback recipe populate a similar region as those from the standard recipe but there are some with significantly lower (only $\sim 10^{3-4}\,{\rm M}_\odot$) cold gas. We have verified that altering the reionization epoch or star formation efficiency does not have a significant impact on the present-day cold gas mass of satellite galaxies. This means that most of the cold gas in satellites was already in place when they were central galaxies, and that this gas has not been affected much by star formation and/or feedback. We recall that in our models, star formation only occurs when the mean surface density of the cold gas is above a certain threshold. Strong supernova feedback can in principle reduce the gas content in the cold phase, but most of the satellites form stars at very low rates, so SN feedback will be less important. In addition, increasing the supernova efficiency would reduce the luminosity (and metallicity) of the model galaxies, ruining the agreement with observational data shown earlier in this study.

It is known that Local Group galaxies show a morphological segregation in the sense that gas-deficient dSphs are closer to the giant spirals (the MW and M31), while the gas-rich dIrrs are more evenly distributed (Mateo 1998). Recent studies, based on deeper HI surveys by Grcevich & Putman (2009) also show that there is a clear correlation between galactocentric distance and HI content for dwarf galaxies in the Local Group. These are interpreted as indications that the Local Group environment influences the gas content of satellites through tidal stripping and ram-pressure stripping (see e.g. Grebel et al. 2003; Mayer et al. 2006). The excessive cold gas associated with our model satellites might be due to our neglecting of gas removal mechanisms, or to a simplified calculation of the surface density threshold (particularly for those satellites which are away from the giant disks, where environment is expected to play a less important role).

3.5 Dark matter halo mass and the dynamical properties

As in Li et al. (2009), we trace the evolution of $V_{\rm max}$ (i.e. the peak circular velocity of the associated dark matter subhalo), $M_{\rm DM}$ and the directly measured $M_{0.6}$ in the last 2 Gyrs for each satellite. 16 out of 51 model satellites are classified as tidally disturbed and these include those two model satellites which have experienced severe tidal stripping, i.e. $M_* > M_{\rm DM}$ at $z = 0$ using our fiducial model. Fig. 12 shows $V_{\rm max}$ as a function of M_V for those 35 model satellites that do not show signs of tidal disturbance. Black circles are for the standard feedback scheme, while grey ones are for the alternative feedback scheme. The latest constraints on $V_{\rm max}$ for 8 classical MW dSphs based on Jeans/MCMC analysis by Walker et al. (2009) are shown as asterisks. Under the assumption of constant velocity anisotropy, their data could constrain $V_{\rm max}$ for Fornax, while only lower limits were derived for the other dSphs (upwards arrows in the Figure). Assuming that classical MW satellites are not tidally disturbed, our models predict that they are associated with dark matter haloes with $V_{\rm max} \gtrsim 10\,{\rm km\,s^{-1}}$, regardless the choice of SN feedback recipe. This is fairly consistent with the constraints by Peñarrubia et al. (2008) and Walker et al. (2009).

Fig. 13 shows the mass-to-light ratios calculated using masses within 0.6 kpc, $M_{0.6}/L$, as a function of absolute magnitude. The luminosities shown are from our fiducial model. The data points for the eight classical MW dSph (i.e. excluding Sgr dSph) measured by Strigari et al. (2007) are overplotted as (blue) asterisks. The lower and middle dashed lines correspond to constant mass values of $M_{0.6} = 6 \times 10^6\,{\rm M}_\odot$ and $M_{0.6} = 7 \times 10^7\,{\rm M}_\odot$ and indicate the upper and lower limits for the observed $M_{0.6}$. For each satellite in our model, two methods can be applied to measure the $M_{0.6}$: 1) to directly sum up bound dark matter particles within 0.6 kpc from the

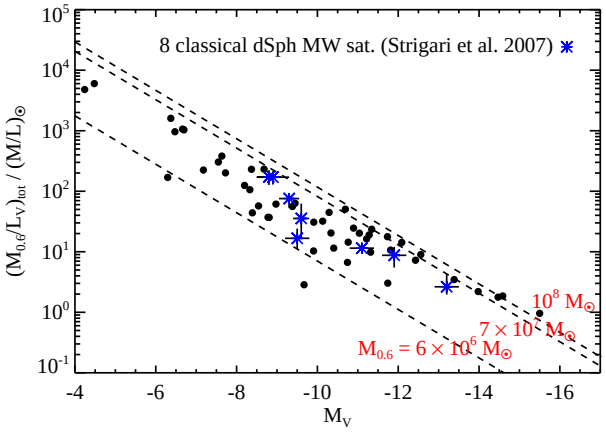

Figure 13. Mass-to-light ratio of 8 Milky Way classical dSphs and model satellites as a function of luminosity. The mass corresponds to the dark matter mass within 0.6 kpc. For the MW dSphs, data are taken from Strigari et al. (2007) and plotted as asterisks. The lower and middle dashed lines correspond to constant values of $M_{0.6} = 6 \times 10^6\,\mathrm{M}_\odot$ and $7 \times 10^7\,\mathrm{M}_\odot$, and mark the upper and lower limits of the measured $M_{0.6}$ for the MW dSphs.

centre of mass[7]; 2) to assume that the inner density profiles are fit by Einasto profiles. Following Li et al. (2009), we compute $M_{0.6}$ by employing the second method for satellites which show signatures of tidal perturbation[8], and use the direct summation method for the other satellites.

Our model predicts that the faintest satellites are the most dark matter dominated, in agreement with observational measurements. It is encouraging that the data points and the model satellites follow a similar trend, and that the spread in the mass-to-light ratio is also comparable. These results can translate into the $M_{0.6}$-L_V plot presented and discussed in Li et al. (2009) and are consistent with the claim that the MW satellites are embedded in dark haloes whose mass is $\sim 10^7\,\mathrm{M}_\odot$ *within the optical extent* as proposed by Mateo (1998), despite the fact that their luminosities span nearly five orders of magnitude (Strigari et al. 2008). The same conclusions hold when we use the luminosities predicted by the alternative feedback scheme, and the only difference is that there are more faint satellites ($M_V > -5$) which have $3,000 < M_{0.6}/L_V < 20,000\,[\mathrm{M/L}]_\odot$.

Datasets which cover large radius as well as internal proper motions for stars in these systems are crucial for drawing further conclusions on the total mass content of the MW satellites. From our modelling of the baryonic physics, we expect a minimum dark matter halo mass of galaxies before accretion onto a MW-like host (equivalent $V_{\rm vir} = 16.7\,\mathrm{km\,s^{-1}}$), introduced by the atomic hydrogen cooling limit (see also the discussion in Section 4.3).

4 DISCUSSION AND IMPLICATIONS

4.1 Number of satellites

Spectra of distant quasars suggest that reionization was completed by $z = 6$ (Fan et al. 2002), yet the exact duration and processes by which the Universe was reionized are not well understood. Our choice of $z_{\rm reio} = 15$ is consistent with the current observational constraints of $z_{\rm reio} = 11.0 \pm 1.4$ given by the *WMAP* 5-year data, which are obtained assuming the reionization occurred instantaneously (Hinshaw et al. 2009). In our model, the suppression of cooling in haloes with $V_{\rm vir} < 16.7\,\mathrm{km\,s^{-1}}$ is the most crucial mechanism which alleviates the discrepancy in the number of surviving dark and luminous satellites. The number of luminous satellites is 1774 in a model that does not take reionization into account and in which haloes with $T_{\rm vir}$ lower than 10^4 K, are able to cool as much gas as a 10^4 K halo with the same metallicity. If cooling is forbidden in these haloes, $N_{\rm sat}$ reduces to 121. In a model that includes only reionization (no suppression of the cooling in small haloes) $N_{\rm sat} = 286$ if $z_{\rm reio} = 8$, and $N_{\rm sat} = 73$ when $z_{\rm reio} = 15$. Forbidding cooling in small haloes, the number of luminous satellites varies from 88 to 51 when changing $z_{\rm reio}$ from 8 to 15. The dependence of $N_{\rm sat}$ on $z_{\rm reio}$ in our model appears slightly stronger than in other recent studies, e.g. by Kravtsov et al. (2004) and Macciò et al. (2009). Both $N_{\rm sat}(z_{\rm reio} = 15)$ and $N_{\rm sat}(z_{\rm reio} = 8)$ from our modelling are, however, consistent with current observational constraints, especially when the possible anisotropic distribution of the satellites is taken into account (Tollerud et al. 2008). The dependence on $z_{\rm reio}$ found in our model appears to be consistent with recent results by Busha et al. (2009).

Recent hydrodynamical simulations of reionization have suggested that the work by Gnedin (2000) might have overestimated the value of the 'filtering mass' (Hoeft et al. 2006; Okamoto et al. 2008). We acknowledge that this could imply that our model may underestimate the number of surviving satellites, especially at low or intermediate luminosities. Macciò et al. (2009) show, however, that effect on the luminosity function of lowering the value of filtering mass can be compensated with an earlier epoch of reionization. We remind the reader that our study could not address the scatter in the luminosity function expected as a result of halo-to-halo variation. Macciò et al. show that the number of satellites changes by about a factor of two in each luminosity bin owing to the variations of merging histories of host galaxies in the mass range of $0.8-1.2\times10^{12}h^{-1}\,\mathrm{M}_\odot$. Their study also suggests that more massive central galaxies (with $M = 2.63 \times 10^{12}h^{-1}\,\mathrm{M}_\odot$) would host a larger number of satellites. These studies can be addressed using new high-resolution simulations of MW-like haloes covering a range of total masses and merging histories (e.g. the Aquarius project, Springel et al. 2008).

Our model does not take into account the loss of stars due to tidal stripping. We have, however, analysed the evolution of the bound dark matter mass ($M_{\rm DM}$) and $M_{0.6}$ for the surviving model satellites, and found that only ~ 10 of them show significant evolution in the last 2 Gyrs. Since baryons are much more concentrated than dark matter, we do not expect this process to affect significantly the luminosity of our satellites.

Another process that we have not included, and which is potentially important for the satellite luminosities is ram pressure stripping of the cold gas. This is likely to be a stronger effect in our fiducial satellite-model than in the *ejection* model, where SN feedback itself is strong enough and thus reduces the cold gas content of satellite galaxies. The impact of ram-pressue on the most luminous satellites is also expected to be weak as these are typically associated with the most massive subhaloes, that were accreted most recently. A more careful modelling that includes how baryons are affected by the interactions with the MW-like galaxy is clearly needed (Mayer et al. 2006).

[7] determined with the 10 per cent most bound particles in each associated subhalo

[8] The two model satellites with $M_* > M_{\rm DM}$ at $z = 0$ are excluded from this analysis.

4.2 Satellites associated with small dark matter haloes and ultra-faint satellites

In our study, we have excluded satellite (Type 2) galaxies whose associated dark matter subhalo was reduced below the resolution limit of the simulation (i.e. $< 2 \times 10^6\,\mathrm{M}_\odot$). In our fiducial satellite-model, there are 72 Type 2 galaxies, that cover a wide range of present day luminosities (similar to that covered by satellites associated with a distinct dark matter substructure but extended to the fainter end). By tracing their position using the most bound particles of their associate subhaloes at the last time they were identified, we find that the median distance of Type 2 galaxies from the host is ~ 20 kpc at $z = 0$. 90 per cent of them are within 120 kpc with a maximum distance of ~ 170 kpc, and they follow a much more centrally concentrated distribution compared to that of Type 1 galaxies (see also Gao et al. 2004). Among those Type 2 galaxies within the inner 20 kpc, about 40 per cent are fainter than $M_V = -5$ at $z = 0$ using the more effective SN feedback scheme. If we were to find the counterparts/remnants of Type 2 galaxies in the observations, they would likely show a disturbed morphology and/or tidal streams and reside very close to the host galaxy. A few ultra-faint satellites which show irregular morphologies might be indicating they are tidally disturbed, e.g. Hercules dSph (Coleman et al. 2007; Sand et al. 2009). However, it is not yet clear whether the irregularities seen in some ultra-faints are indeed owing to tidal interactions given the scarce of stars currently observed (Martin et al. 2008).

The luminosity function predicted by our model is in good agreement with the power-law-shaped 'all-sky' SDSS luminosity function, especially when using the more efficient SN feedback scheme. However, this model underestimates the number of expected ultra-faint (fainter than $M_V = -5$) satellites (see Fig. 4 right panel). Recent theoretical studies have proposed that the ultra-faint satellites are those fossil satellites which formed before reionization and managed to cool some gas via H_2 (Bovill & Ricotti 2009; Salvadori & Ferrara 2009; Muñoz et al. 2009). In Fig. 14, we show the luminosity functions with three different models all using our *ejection* SN feedback scheme. The lightest histogram shows results obtained using $z_{\rm reio} = 8$ and allowing haloes with $T_{\rm vir} < 10^4$ K to cool as much gas as a $T_{\rm vir} = 10^4$ K halo of the same metallicity. The intermediate histogram adopts the same assumption for cooling in small haloes but assumes $z_{\rm reio} = 12$. The thickest histogram also adopts $z_{\rm reio} = 12$ but forbids cooling in small haloes. The two models using $z_{\rm reio} = 12$ agree well with each other except at the faint end (as expected). So shutting down cooling in small haloes mostly affects the luminosity function fainter than $M_V = -5$. If some of those small haloes could have cooled via molecular hydrogen, they would indeed populate the ultra-faint satellites regime. However, it should be noted that, when adopting $z_{\rm reio} = 12$, there is still a non negligible fraction (about 20 per cent) of ultra-faint satellites that are associated with haloes with $T_{\rm vir} > 10^4$ K and whose low luminosities are driven by the very efficient SN feedback.

4.3 Which dark matter substructures can form stars?

Fig. 1 shows that the mass range $10^8 - 10^9\,\mathrm{M}_\odot$ is populated with subhaloes both with and without stars in the fiducial model. It is interesting to ask why some massive subhaloes have failed to form stars. To address this question, we trace the evolution of the dark matter mass M_{200} for all satellites and store the maximum mass and epoch ($t = tm$) when this is reached. Fig. 15 shows the maximum mass against the present-day (bound) mass $M_{\rm DM}$. Luminous

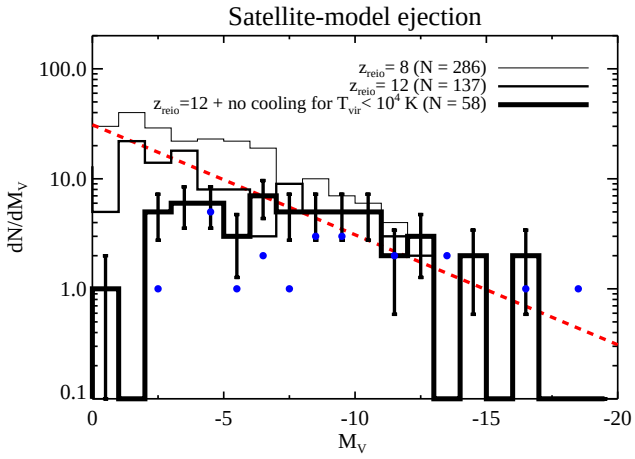

Figure 14. Luminosity functions for the MW satellites (dashed-line and points) and for our model satellites using the more efficient supernova feedback scheme (solid histograms). Data are the same as those in Fig. 3.

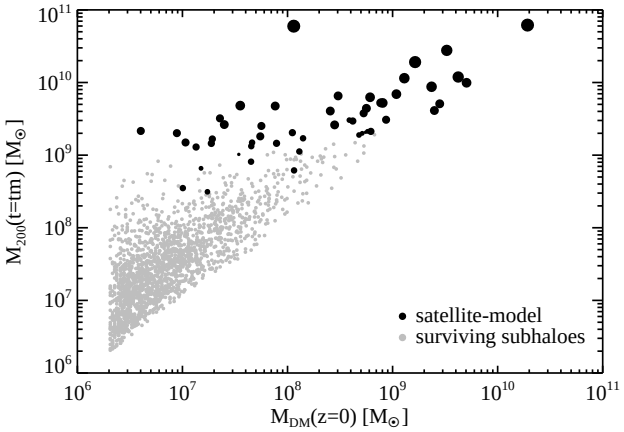

Figure 15. Maximum M_{200} mass against present-day bound dark matter mass for luminous (black) and dark (grey) satellites. The symbol size for the luminous satellites increases with the luminosity as given by the satellite-model.

satellites are shown in black and dark satellites in grey. The symbol size for the satellites increases with the luminosity as predicted by the fiducial satellite-model. It is clear that most of the subhaloes associated with the luminous satellites were once much more massive, and that the most luminous satellites are on average embedded within the most massive subhaloes at present-day (see also Fig. 6). On the other hand, dark satellites (in this mass range) have present-day masses similar to their peak values (see also Kravtsov et al. 2004). It is also clear that model satellites have a wide range of peak M_{200} prior to their accretions onto the central galaxy.

We plot the maximum mass as a function of the redshift when this value was reached in Fig. 16. The minimum mass defined by the cooling via atomic hydrogen as a function of redshift is indicated by the solid curve. The Figure shows that most of the dark satellites were below the threshold and not able to cool gas, even when they reached their peak mass. In contrast, luminous satellites live in subhaloes which have been massive enough and managed to have sufficient cold gas to fuel star formation. We also notice that no luminous satellites achieved their maximum mass before $z = 6$.

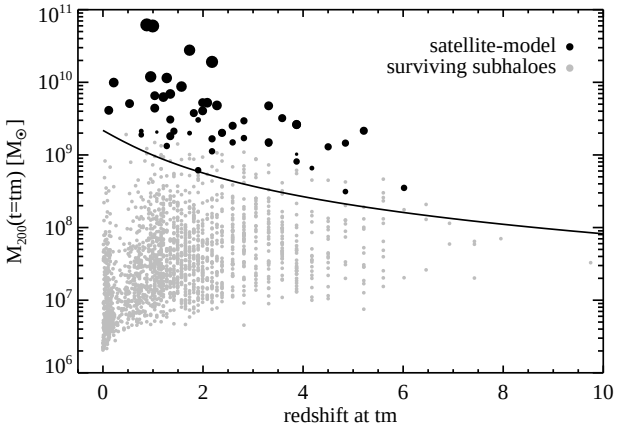

Figure 16. Maximum M_{200} mass as a function of the redshift when it was reached for luminous (black) and dark (grey) satellites. The minimum mass for cooling via atomic hydrogen at each redshift is indicated by the solid line. Symbols are the same as in Fig. 15.

We have also checked when and where the present-day luminous satellites typically formed in the simulation. We find that the surviving satellites were all detected in the simulation early, namely their $M_{\rm DM}$ exceeded $2 \times 10^6\,{\rm M}_\odot$ around the epoch of reionization ($z_{\rm reio} = 15$ in the satellite-model) and mostly before the end of reionization ($z = 11$), while the dark ones have emerged throughout the Hubble time. The distance of the model satellites to the MW-like galaxy at emergence is typically around ~ 100 kpc.

Font et al. (2006) suggest that surviving satellites were accreted up to 9 Gyr ago and therefore have been through a different chemical enrichment history compared to those that were accreted very early on and contributed to the stellar halo. In our model there are a few objects that became satellites more than 10 Gyr ago and have survived the tidal interactions with the MW-halo (see Fig. 6 and Fig. 8). Typically, however, their peak masses are smaller than those of the objects that contributed significantly to the build up of the stellar halo (De Lucia & Helmi 2008). It is possible to envision the building blocks of the stellar halo as the most massive satellites that existed at early times, i.e. the counterparts of the very faint ones, whose orbits did not decay via dynamical friction, and hence have generally been more sheltered from the tidal forces of the Galaxy.

5 CONCLUSIONS

We use a hybrid model of galaxy formation and evolution to study the satellites of the Milky Way in a cosmological context. Our method combines high resolution N-body simulations which allow us to trace the evolution and the dynamics of dark matter haloes directly, and phenomenological prescriptions to follow the evolution of baryons. Our adopted semi-analytical recipes and values for the relevant parameters result in models that reproduce the properties of galaxies on large scales as well as those of the MW. A few modifications were needed, however, to reproduce the observational properties of the MW satellites.

With the presence of a reionization background that reduces the baryon content of subhaloes around $z = 15$ and the suppression of cooling for haloes with $V_{\rm vir} < 16.7\,{\rm km\,s^{-1}}$, our model can reproduce the total number and the luminosity function observed for the satellites of the MW. Our fiducial SA model also shows good agreement with the metallicity distribution and the metallicity-luminosity relation when a large fraction of newly formed metals in small galaxies are recycled through its hot component and with other properties shared by the MW satellites, e.g. the radial distribution, luminosity-size relation and the star formation histories. However, our fiducial model produces an excess of satellites with $M_V \sim -10$ and $\log(Z_*/\,{\rm Z}_\odot) \sim -1$, and does not predict ultra-faint satellites with the total luminosity below $L_V \sim 10^{4.5}\,{\rm L}_\odot$.

We have tested an alternative SN feedback recipe which is stronger for galaxies with $V_{\rm vir} \lesssim 90\,{\rm km\,s^{-1}}$ compared to the standard feedback recipe. With this alternative feedback recipe, our model predicts the same number of surviving satellites (which populate the same set of subhaloes as the standard feedback model). The alternative feedback model predicts more satellites with $M_V < -5$ which also follow the metallicity-luminosity relation traced by the classical and the ultra-faint SDSS MW satellites (Kirby et al. 2008) down to ${\rm [Fe/H]} \sim -2.5$ and $L_V \sim 10^3\,{\rm L}_\odot$.

Our model satellites are embedded in dark matter haloes with innermost masses within 600 pc between $6 \times 10^6\,{\rm M}_\odot$ and $7 \times 10^7\,{\rm M}_\odot$, in very good agreement with the estimates for the classical MW dSphs derived by Strigari et al. (2007). This demonstrates that the existence of a common scale for the innermost mass is a natural outcome of the CDM galaxy formation and evolution model (see also Li et al. 2009; Macciò et al. 2009; Koposov et al. 2009). Satellites are dark matter dominated even within the optical extent, and the mass-to-light ratio increases with decreasing luminosity. Surviving satellites in our model are associated with ancient haloes which had masses of a few $10^6\,{\rm M}_\odot$ by $z \sim 10 - 20$, and acquired their maximum dark matter mass after $z \sim 6$.

The brightest satellites in our model are associated with the most massive subhaloes, were accreted later ($z \lesssim 1$) and show extended star formation histories, with only 1 per cent of their stars made by the end of the reionization (lookback time ~ 13 Gyr). On the other hand, the fainter satellites tend to be accreted early on, are all dominated by stars with age > 10 Gyr, and a few of them are dominated by stars formed before the reionization was complete. In our models, the classical MW satellites are associated with dark matter subhaloes with a peak circular velocity $\gtrsim 10\,{\rm km\,s^{-1}}$, in agreement with the recent results by Walker et al. (2009).

Although our model satellites are in very good agreement with the latest observations in terms of luminosity, metallicity and the innermost dark matter content, the agreement with the ultra-faint galaxies is less conclusive. Note that the alternative feedback recipe seems to give a better fit to the properties of ultra-faint satellites. This could imply that the ultra-faint satellites of the MW are associated with dark matter haloes with lower $V_{\rm vir}$ compared to the classical ones (i.e. they are more sensitive to SN feedback). However, until we properly model the loss of baryons due to tidal stripping and ram pressure in these small systems, and until we obtain more observational constraints on these objects, their nature will probably remain unclear.

ACKNOWLEDGEMENTS

We thank Felix Stoehr for making his simulations available; Eline Tolstoy, Scott Trager and Simon White for useful comments on an early version of this manuscript. The referee, Alexander Knebe, is warmly thanked for a careful reading and suggestions to improve the presentation of the manuscript. Y-SL is grateful to the Netherlands Foundation for Scientific Research (NWO), Leids

Kerkhoven-Bosscha Fonds (LKBF) and MPA for the financial support to visit MPA. GDL acknowledges financial support from the European Research Council under the European Community's Seventh Framework Programme (FP7/2007-2013)/ERC grant agreement n. 202781. This work was supported by a VIDI grant to AH from NWO. The computing support and hospitality of MPA are also acknowledged for the contributions to this work. This research has made use of NASA's Astrophysics Data System Service.

REFERENCES

Babul A., Rees M. J., 1992, MNRAS, 255, 346
Battaglia G., et al. 2005, MNRAS, 364, 433
Battaglia G., Irwin M., Tolstoy E., Hill V., Helmi A., Letarte B., Jablonka P., 2008, MNRAS, 383, 183
Baugh C. M., 2006, Reports of Progress in Physics, 69, 3101
Belokurov V., et al. 2006, ApJ, 647, L111
Belokurov V., et al. 2007, ApJ, 654, 897
Belokurov V., et al. 2008, ApJ, 686, L83
Belokurov V., et al. 2009, MNRAS, 397, 1748
Benson A. J., Frenk C. S., Lacey C. G., Baugh C. M., Cole S., 2002, MNRAS, 333, 177
Bovill M. S., Ricotti M., 2009, ApJ, 693, 1859
Brüns C., et al. 2005, A&A, 432, 45
Bullock J. S., Kravtsov A. V., Weinberg D. H., 2000, ApJ, 539, 517
Busha M. T., Alvarez M. A., Wechsler R. H., Abel T., Strigari L. E., 2009, submitted to ApJ (ArXiv e-prints:0901.3553)
Cole A. A., 2001, ApJ, 559, L17
Coleman M. G., et al. 2007, ApJ, 668, L43
Croton D. J., et al. 2006, MNRAS, 365, 11
De Lucia G., Blaizot J., 2007, MNRAS, 375, 2
De Lucia G., Helmi A., 2008, MNRAS, 391, 14
De Lucia G., Kauffmann G., Springel V., White S. D. M., Lanzoni B., Stoehr F., Tormen G., Yoshida N., 2004, MNRAS, 348, 333
De Lucia G., Kauffmann G., White S. D. M., 2004, MNRAS, 349, 1101
Dekel A., Silk J., 1986, ApJ, 303, 39
Diemand J., Kuhlen M., Madau P., 2007, ApJ, 657, 262
Dolphin A. E., Weisz D. R., Skillman E. D., Holtzman J. A., 2005, ArXiv Astrophysics e-prints:astro-ph/0506430
Fan X., Narayanan V. K., Strauss M. A., White R. L., Becker R. H., Pentericci L., Rix H.-W., 2002, AJ, 123, 1247
Font A. S., Johnston K. V., Bullock J. S., Robertson B. E., 2006, ApJ, 638, 585
Gao L., De Lucia G., White S. D. M., Jenkins A., 2004, MNRAS, 352, L1
Gao L., White S. D. M., Jenkins A., Stoehr F., Springel V., 2004, MNRAS, 355, 819
Ghez A. M., et al. 2008, ApJ, 689, 1044
Gnedin N. Y., 2000, ApJ, 542, 535
Grcevich J., Putman M. E., 2009, ApJ, 696, 385
Grebel E. K., Gallagher III J. S., Harbeck D., 2003, AJ, 125, 1926
Haiman Z., Abel T., Rees M. J., 2000, ApJ, 534, 11
Harbeck D., et al. 2001, AJ, 122, 3092
Helmi A., et al. 2006, ApJ, 651, L121
Hinshaw G., et al. 2009, ApJS, 180, 225
Hoeft M., Yepes G., Gottlöber S., Springel V., 2006, MNRAS, 371, 401
Irwin M. J., et al. 2007, ApJ, 656, L13
Kamionkowski M., Liddle A. R., 2000, Physical Review Letters, 84, 4525
Kauffmann G., Haehnelt M., 2000, MNRAS, 311, 576
Kauffmann G., White S. D. M., Guiderdoni B., 1993, MNRAS, 264, 201
Kirby E. N., Simon J. D., Geha M., Guhathakurta P., Frebel A., 2008, ApJ, 685, L43
Klypin A., Kravtsov A. V., Valenzuela O., Prada F., 1999, ApJ, 522, 82
Koch A., et al. 2009, ApJ, 690, 453
Koch A., Grebel E. K., Kleyna J. T., Wilkinson M. I., Harbeck D. R., Gilmore G. F., Wyse R. F. G., Evans N. W., 2007, AJ, 133, 270
Koch A., Wilkinson M. I., Kleyna J. T., Gilmore G. F., Grebel E. K., Mackey A. D., Evans N. W., Wyse R. F. G., 2007, ApJ, 657, 241
Koposov S., et al. 2008, ApJ, 686, 279
Koposov S. E., Yoo J., Rix H.-W., Weinberg D. H., Macciò A. V., Escudé J. M., 2009, ApJ, 696, 2179
Kravtsov A. V., Gnedin O. Y., Klypin A. A., 2004, ApJ, 609, 482
Larson R. B., 1974, MNRAS, 169, 229
Li Y.-S., Helmi A., 2008, MNRAS, 385, 1365
Li Y.-S., Helmi A., De Lucia G., Stoehr F., 2009, MNRAS, 397, L87
Mac Low M.-M., Ferrara A., 1999, ApJ, 513, 142
Macciò A. V., Kang X., Fontanot F., Somerville R. S., Koposov S. E., Monaco P., 2009, ArXiv e-prints:0903.4681
Macciò A. V., Kang X., Moore B., 2009, ApJ, 692, L109
Martin N. F., de Jong J. T. A., Rix H.-W., 2008, ApJ, 684, 1075
Mateo M., Olszewski E. W., Pryor C., Welch D. L., Fischer P., 1993, AJ, 105, 510
Mateo M. L., 1998, ARA&A, 36, 435
Mayer L., Mastropietro C., Wadsley J., Stadel J., Moore B., 2006, MNRAS, 369, 1021
Moore B., Ghigna S., Governato F., Lake G., Quinn T., Stadel J., Tozzi P., 1999, ApJ, 524, L19
Muñoz J. A., Madau P., Loeb A., Diemand J., 2009, ArXiv e-prints:0905.4744
Muñoz R. R., Carlin J. L., Frinchaboy P. M., Nidever D. L., Majewski S. R., Patterson R. J., 2006, ApJ, 650, L51
Navarro J. F., Frenk C. S., White S. D. M., 1997, ApJ, 490, 493
Okamoto T., Gao L., Theuns T., 2008, MNRAS, 390, 920
Orban C., Gnedin O. Y., Weisz D. R., Skillman E. D., Dolphin A. E., Holtzman J. A., 2008, ApJ, 686, 1030
Peñarrubia J., McConnachie A. W., Navarro J. F., 2008, ApJ, 672, 904
Ryan-Weber E. V., Begum A., Oosterloo T., Pal S., Irwin M. J., Belokurov V., Evans N. W., Zucker D. B., 2008, MNRAS, 384, 535
Salvadori S., Ferrara A., 2009, MNRAS, 395, L6
Sand D. J., Olszewski E. W., Willman B., Zaritsky D., Seth A., Harris J., Piatek S., Saha A., 2009, ApJ, 704, 898
Simon J. D., Geha M., 2007, ApJ, 670, 313
Smith M. C., et al. 2007, MNRAS, 379, 755
Somerville R. S., 2002, ApJ, 572, L23
Spergel D. N., et al. 2007, ApJS, 170, 377
Springel V., Wang J., Vogelsberger M., Ludlow A., Jenkins A., Helmi A., Navarro J. F., Frenk C. S., White S. D. M., 2008, MNRAS, 391, 1685
Springel V., White S. D. M., Tormen G., Kauffmann G., 2001, MNRAS, 328, 726

Springel V., Yoshida N., White S. D. M., 2001, New Astronomy, 6, 79
Stoehr F., 2006, MNRAS, 365, 147
Stoehr F., White S. D. M., Tormen G., Springel V., 2002, MNRAS, 335, L84
Strigari L. E., Bullock J. S., Kaplinghat M., Diemand J., Kuhlen M., Madau P., 2007, ApJ, 669, 676
Strigari L. E., Bullock J. S., Kaplinghat M., Simon J. D., Geha M., Willman B., Walker M. G., 2008, Nature, 454, 1096
Sutherland R. S., Dopita M. A., 1993, ApJS, 88, 253
Tollerud E. J., Bullock J. S., Strigari L. E., Willman B., 2008, ApJ, 688, 277
van den Bergh S., 2000, The Galaxies of the Local Group. Cambridge University Press, Cambridge, UK, 2000 Cambridge Astrophysics Series, vol no: 35, ISBN: 0521651816.
Walker M. G., Belokurov V., Evans N. W., Irwin M. J., Mateo M., Olszewski E. W., Gilmore G., 2009, ApJ, 694, L144
Walker M. G., Mateo M., Olszewski E. W., Peñarrubia J., Wyn Evans N., Gilmore G., 2009, ApJ, 704, 1274
Walsh S. M., Jerjen H., Willman B., 2007, ApJ, 662, L83
Westerlund B. E., 1997, The Magellanic Clouds. Cambridge University Press, Cambridge, UK, 1997 Cambridge Astrophysics Series, vol no: 29, ISBN: 0521480701.
White S. D. M., Frenk C. S., 1991, ApJ, 379, 52
White S. D. M., Rees M. J., 1978, MNRAS, 183, 341
Willman B., et al. 2005a, AJ, 129, 2692
Willman B., et al. 2005b, ApJ, 626, L85
Xue X. X., et al. 2008, ApJ, 684, 1143
Zentner A. R., Bullock J. S., 2003, ApJ, 598, 49
Zucker D. B., et al. 2006a, ApJ, 650, L41
Zucker D. B., et al. 2006b, ApJ, 643, L103

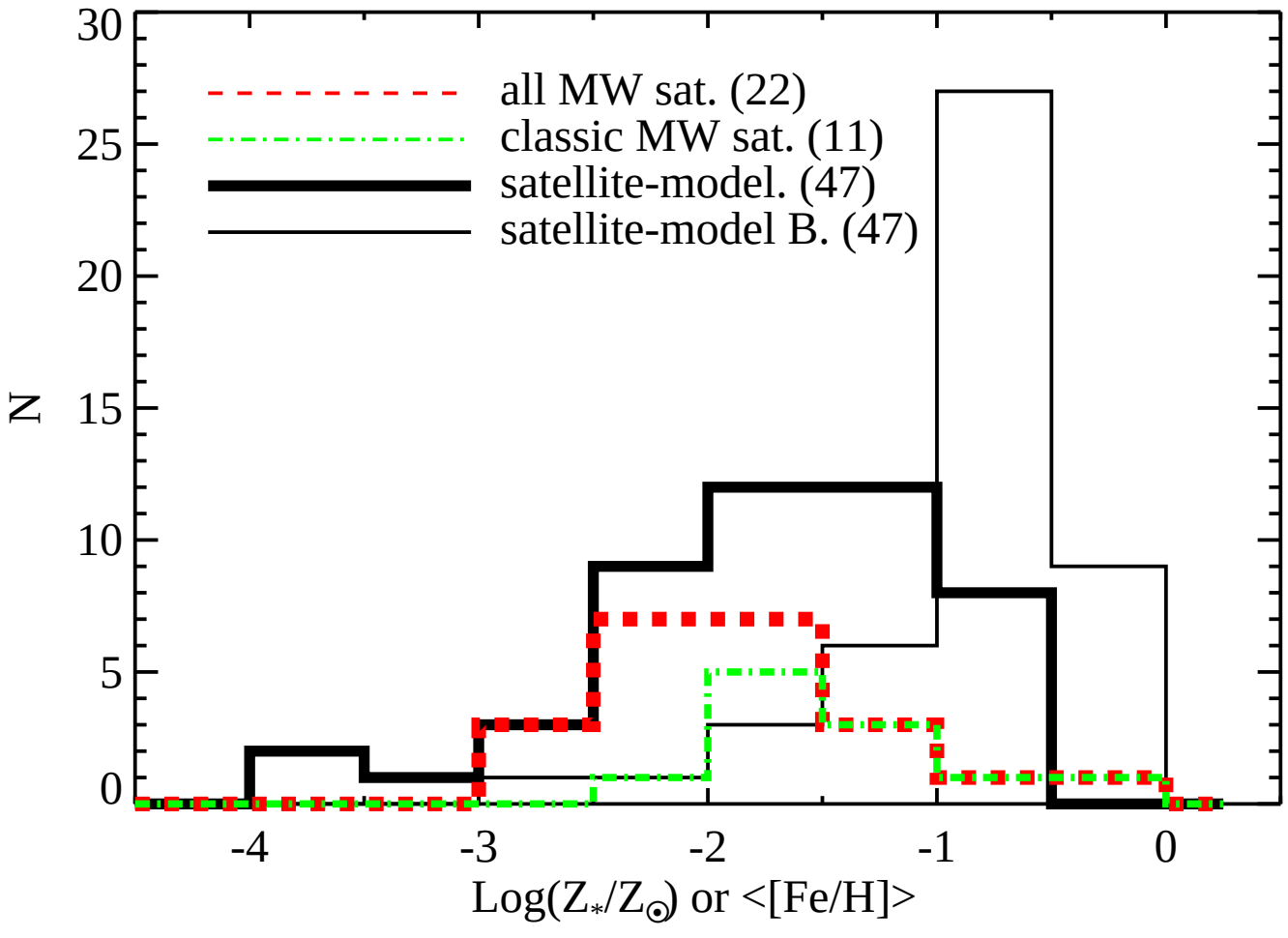
all MW sat. (22)
classic MW sat. (11)
satellite-model. (47)
satellite-model B. (47)
N
30
25
20
15
10
5
0
-4
-3
-2
-1
0
Log(Z*/Z⊙) or <[Fe/H]>